

MODELING OF ECLIPSING BINARY STAR SYSTEMS NSVS 5060083

AND NSVS 5354761

A THESIS

SUBMITTED TO THE GRADUATE SCHOOL

IN PARTIAL FULFILLMENT OF THE REQUIREMENTS

FOR THE DEGREE

MASTER OF SCIENCE

BY

MICHAEL HOLCOMB

DR. ROBERT BERRINGTON - ADVISOR

BALL STATE UNIVERSITY

MUNCIE, INDIANA

DECEMBER 2016

## Table of Contents

Table of Contents	2
List of Figures	3
List of Tables	5
Abstract	6
Chapter 1: Introduction	8
1.1 Eclipsing Binary Star System Background Information	8
1.2 Eclipsing Binary Star System Classification	11
1.3 Northern Sky Variability Survey	16
Chapter 2: Observations	17
Chapter 3: Data Reduction and Analysis	20
Chapter 4: Modeling with PHOEBE	32
Chapter 5: Results	36
5.1 NSVS 5354761	36
5.2 NSVS 5060083	41
Chapter 6: Conclusions	51
Acknowledgements	53
References	54

## Figures

Figure 1: Graphical Explanation of Inclination Angle	8
Figure 2: Example of an Eclipsing Binary Star System	9
Figure 3: Examples of three different types of eclipsing binary star systems and their corresponding light curves	12
Figure 4: Display of Equipotential Surfaces About Binary Star Systems	14
Figure 5: Examples of Roche Lobe Classification	15
Figure 6: Star field for NSVS 5060083	25
Figure 7: Star Field for NSVS 5354761	26
Figure 8: Observational Date When Inserted into PERANZO	29
Figure 9: Periodogram Example from PERANZO for NSVS 5354761	29
Figure 10: Example of a PERANZO Constructed Light Curve	30
Figure 11: (B-V) Graph for NSVS 5060083.	34
Figure 12: (B-V) Graph for NSVS 5354761	35
Figure 13: Folded Light Curve in Johnson B for NSVS 5354761	38
Figure 14: Residuals for Folded Light Curve in Johnson B Filter	38
Figure 15: Folded Light Curve in Johnson V for NSVS 5354761	39
Figure 16: Residuals for Folded Light Curve in Johnson V Filter	39
Figure 17: Folded Light Curve in Cousins R for NSVS 5354761	40
Figure 18: Residuals for Folded Light Curve in Cousins R Filter	40
Figure 19: Three Dimensional Models of NSVS 5354761	41
Figure 20: Erroneous Modeling of NSVS 5060083	44

Figure 21: Folded Light Curve in Johnson B Filter With Starspots for NSVS 5060083	44
Figure 22: Residuals for Folded Light Curve in Johnson B With Spots	45
Figure 23: Folded Light Curve in Johnson V Filter With Starspots for NSVS 5060083	45
Figure 24: Residuals for Folded Light Curve in Johnson V With Spots	46
Figure 25: Folded Light Curve in Cousins R Filter With Starspots for NSVS 5060083	46
Figure 26: Residuals for Folded Light Curve in Cousins R With Spots	47
Figure 27: Three Dimensional Models of NSVS 5060083	47
Figure 28: Folded Light Curve in Johnson B Filter Without Starspots For NSVS 5060083	48
Figure 29: Residuals for Folded Light Curve in Johnson B Without Spots	48
Figure 30: Folded Light Curve in Johnson V Filter Without Starspots for NSVS 5060083	49
Figure 31: Residuals for Folded Light Curve in Johnson V Without Spots	49
Figure 32: Folded light curve in Cousins R filter without starspots for NSVS 5060083	50
Figure 33: Residuals for Folded Light Curve in Cousins R Without Spots	50

## Tables

Table 1: Observational Data For NSVS 5060083	19
Table 2: Observational Data For NSVS 5354761	19
Table 3: Celestial Coordinates and Designations of Target and Comparison Stars for NSVS 5060083 Star Field	26
Table 4: Celestial Coordinates and Designations of Target and Comparison Stars for NSVS 5354761 Star Field.	27
Table 5: Final Results from the Modeling of NSVS 5060083 and NSVS 5354761	51

## Abstract

**THESIS:** Modeling of Eclipsing Binary Star Systems NSVS 5060083 and NSVS

5354761

**STUDENT:** Michael Holcomb

**DEGREE:** Master of Science

**COLLEGE:** Science and Humanities

**DATE:** December 2016

**Pages:** 54

I present modeling of two eclipsing binary star systems. We define a binary star system as a system whose individual stellar components are gravitationally bound together. My purpose is to model these systems using the software suite entitled Physics of Eclipsing Binaries (PHOEBE), which uses the Wilson-Devinney code. All of the systems I am looking at are part of the Northern Sky Variability Survey (NSVS). The NSVS catalog is a large-area survey generated using observations from April 1999 to March 2000 covering the sky northward of  $\delta > -38^\circ$  declination. The data used to generate the NSVS was taken using the first generation Robotic Optical Transient Search Experiment (ROTSE-I). The imaging system for ROTSE-I has a wide, unfiltered spectral response that covers the wavelengths from B to I of the Johnson-Cousins system.

The intent of the NSVS was to search for variable star systems over a wide area of the sky and it succeeded in discovering many such systems. I purposefully targeted systems that have not been extensively studied and have short orbital periods ( $\sim 12$  hours). Due to the large area of the sky covered by the NSVS, time resolutions for these systems are poor, ( $\sim 24$  hours). For systems whose orbital periods vary on the order of hours rather

than days, finer time resolutions are necessary to complete an extensive photometric study. I targeted and examined two of these systems with much finer time resolutions, (~a few minutes) in order to accurately determine their stellar orbital parameters.

I present observations taken in the three band-pass filters Johnson B and V and Cousins R. The observations of these binary star systems were carried out using both the 0.4 m and 0.6 m telescopes at the Ball State University Observatory located on the rooftop of the Cooper Science building as well as the Southeastern Astronomical Research Association's (SARA) 0.9 m telescope located at the Kitt Peak National Observatory in Arizona. All light curves generated from this data were modeled using the PHOEBE software suite. This analysis allowed me to determine several of the orbital parameters of each system, which can be used as a baseline in future studies.

## Chapter 1: Introduction

The observation of stellar objects is an important part of astronomical research. Much can be learned from these objects. Binary star systems have an advantage over single star systems in that the interactions between the two stars in the binary system can be observed and modeled. This allows the observer to determine, with a reasonable degree of accuracy, several of the parameters of the system.

### 1.1: Eclipsing Binary Star Systems

The two stellar objects in a binary system are gravitationally bound to one another, which causes them to orbit around a common center of mass. Every binary star system has an inclination angle associated with it. The inclination angle of the system is the angle between the plane of the orbits of the stars and the plane of the sky (Percy 2007). An inclination of  $0^\circ$  means that we are looking at the orbital plane of the star system perpendicular to the plane of its orbit. An inclination of  $90^\circ$  means that we are looking at the orbital plane edge on. A graphical example of inclination can be seen in Figure 1.

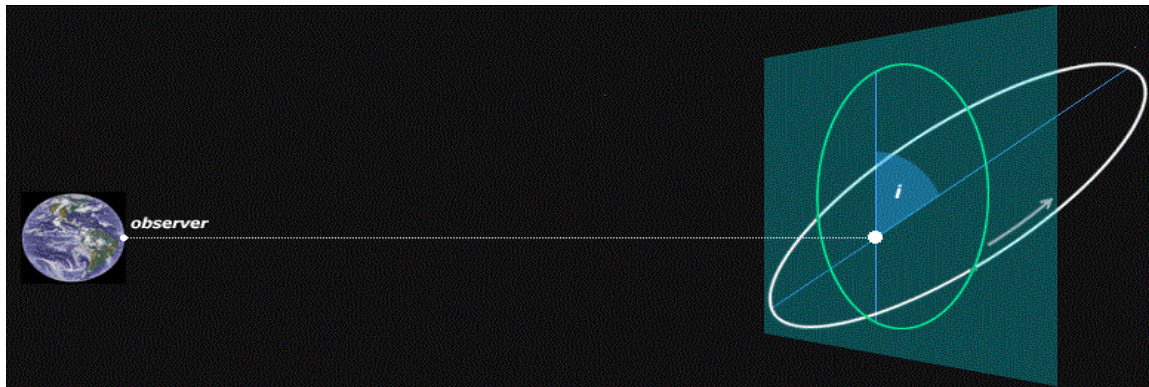


**Figure 1:** Graphical explanation of inclination angle. An inclination of  $0^\circ$  can be seen as the green orbit. An inclination of angle,  $i$ , can be seen as the white orbit. While the teal square is the plane of the orbit at  $0^\circ$  when it is tangent to the celestial sphere ([www.handprint.com/ASTRO/bineye2.html](http://www.handprint.com/ASTRO/bineye2.html)).

Much of the time the orientation of the orbital plane of the system with respect to the Earth is not close to this  $90^\circ$  value. But in some situations it is close enough to  $90^\circ$  that

one of the stars passes between the Earth and its companion eclipsing the companion. When this happens we call the system an eclipsing binary star system. Through examination of such eclipsing binary star systems we can extract several of the systems stellar parameters including the systems mass ratio, orbital period, orbital inclination, and stellar temperatures. An example of an eclipsing binary star system can be seen in Figure 2.

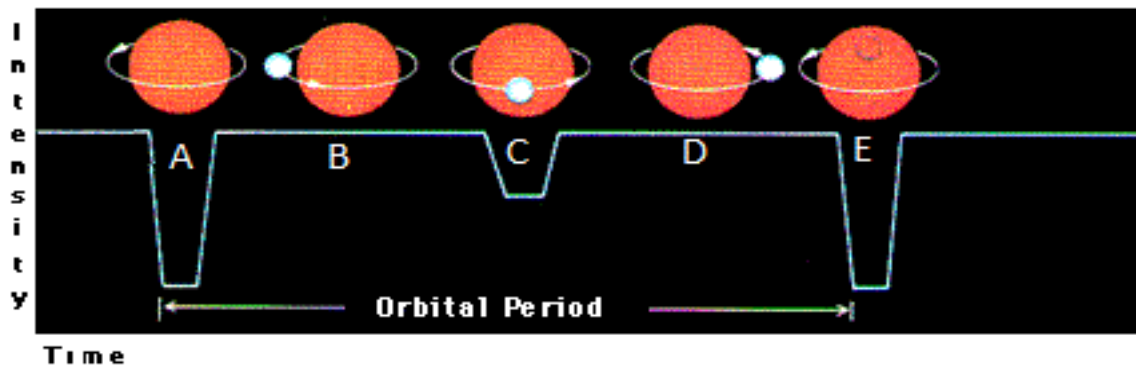


**Figure 2:** Example of an eclipsing binary star system. *Top:* A full eclipse of the smaller star by the larger star can be seen at points A and E. A partial eclipse of the larger star by the smaller star can be seen at point C. *Bottom:* Example light curve for an eclipsing binary star system showing how its flux intensity changes over time. A full orbital period can be seen from left to right with a phase of 0, 0.25, 0.5, 0.75, and back to 0 at points A,B,C,D, and E respectively. (www.nasa.gov).

For eclipsing binary star systems, the closer the inclination angle is to  $90^\circ$ , the longer the eclipse will last and the greater the chance for a full eclipse. A full eclipse can occur when one of the stars in the binary pair passes directly between the Earth and the other star blocking it from sight entirely for a length of time. The eclipses also last for longer at inclinations close to  $90^\circ$  as each star must cross the entire diameter of the other as the eclipses occur. When one of the stars has a smaller radius than the other a full eclipse of the smaller star by the larger one occurs. When the stars are reversed a partial

eclipse of the larger star by the smaller one occurs as only a portion of the larger star is blocked from view.

A method then needs to be found to be able to determine when each particular star in the binary pair is being eclipsed by the other and which orientation of the stellar system gives a particular data result. In order to do this the light curve of the stellar system is examined. A light curve is a measurement of the brightness of the stellar system over time. An example light curve can be seen in Figure 2. It can be seen that over time the intensity of the flux of the stellar system changes over time. It decreases each time an eclipse occurs and the surface of a star is blocked from sight.

If the system has a constant magnitude then the light curve will be just a horizontal line within the error boundaries. This result means that the stellar system is non-variable. For example, a binary star system that is non-eclipsing, i.e. has a low angle of inclination with respect to the Earth, will be non-variable unless there are other variability causing effects that occur within the stellar system such as pulsation or cataclysmic explosive effects.

Taking another look at the sample light curve of an eclipsing binary star system in Figure 1 two eclipses are observed over one orbital period. The eclipse where the brightness of the system decreases the most is called the primary eclipse. The eclipse where the brightness still decreases but by a smaller amount is labeled the secondary eclipse. A primary eclipse occurs when a brighter star passes behind and is eclipsed by a dimmer star. A secondary eclipse occurs when the positions of the two stars are reversed and the dimmer star passes behind and is eclipsed by the brighter star (Percy 2007).

## 1.2: Eclipsing Binary Star System Classification

There are several different subsets of eclipsing binary star systems depending on how the stellar components within the system interact and the age of the system. Exact classification of each binary star system is complex. There are two common ways to classify these binary star systems. The first depends on the light curve of the system, while the second depends on how the stars fill their individual Roche Lobes. A description of what a Roche Lobe is and how they relate to stars will be given later in this thesis.

However, there are many binary star systems that have light curves that do vary over time. The light curve is one way of classifying such systems. With an eclipsing binary star systems the light flux changes over time mainly because of the primary and secondary eclipses. However, other effects such as the presence of starspots or an accretion disk can still influence the light curve. Both of these effects will be discussed later in this thesis. When an eclipse occurs the light flux dips as the brightness of the system decreases. The lowest part of this dip is called the minima. There is a minima for both the primary and the secondary eclipse. The maxima of the light curve is the point where the brightness of the star system is at its highest value.

There are three main classifications that can be made when looking at the light curves of eclipsing binary star systems. These classifications are Algol (EA), Beta Lyrae (EB), and W Ursa Majoris (EW). Examples of these three types of eclipsing binary star systems and their light curves can be seen in Figure 3. It is important to note that the classifications given here are general classifications. There are some exceptions to the general classifications given here for each type of stellar system, but generally they hold true. Algol systems have flat topped maxima, but well-defined eclipses where the primary

and secondary eclipses are of different depths. Beta Lyrae systems have continuously changing light curves with both rounded maxima and minima with the primary and secondary minima again being of different depths. W Ursa Majoris light curves also change continuously but the depth of the minima tend to be equal to each other.

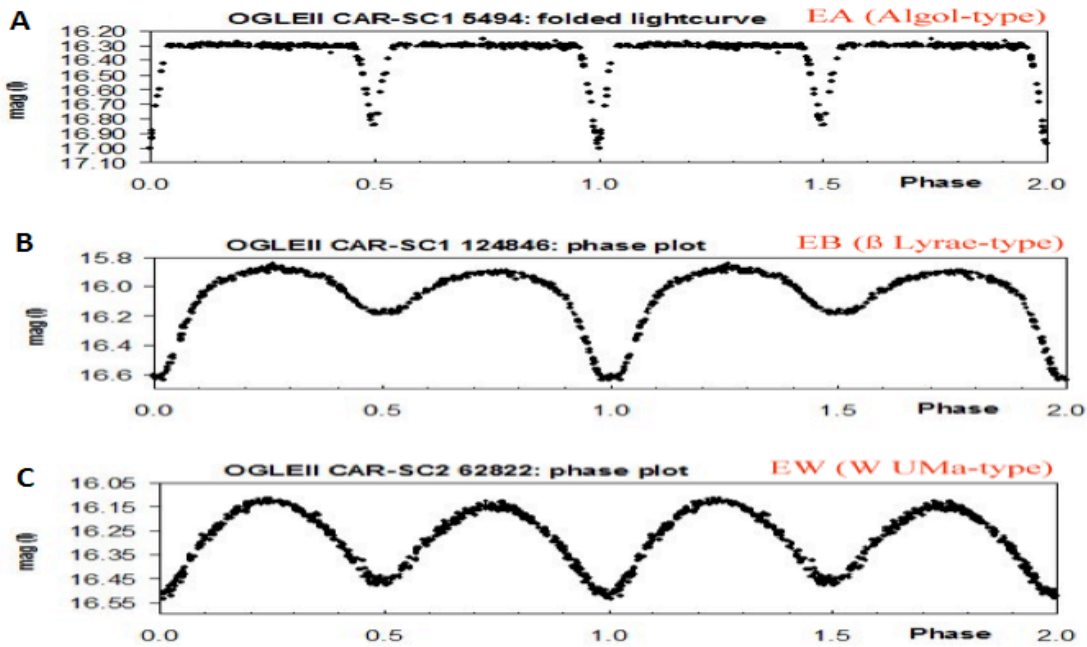


**Figure 3:** Examples of three different types of eclipsing binary star systems and their corresponding light curves. Created from OGLE-II data (Szymanski , 2005) and taken from Hummerich and Bernhard (2012). Light curve A is an example of an Algol type eclipsing binary star system with its flat-topped maxima and well defined eclipses of differing depths. Light curve B is an example of a Beta Lyrae type eclipsing binary star system with its continuously changing light curve with rounded maxima and minima and eclipses of differing depths. Light curve C is an example of a W Ursa Majoris type eclipsing binary star system with its continuously changing light curve but with eclipses of similar depths. (<http://www.vs-compas.belastro.net/bulletin/issue/2/p6>).

Differences in the depths of the minima for the light curves are primarily due to temperature differences between the primary and secondary stars (Percy 2007). Depending on which star is being eclipsed more or less of the combined flux of the system is being eclipsed. With the primary eclipses causing more of the combined flux to be blocked at that point. For W Ursa Majoris systems the difference in temperature between the two stars tends to be small since the stars share a common stellar convective envelope.

Ideally, the two stars will eventually equalize in temperature through thermodynamical processes (Percy 2007). This is why the depths of the primary and secondary minima in W Ursa Majoris type systems tend to be relatively equal. However, with Algol and especially Beta Lyrae systems there can be a large difference in the temperatures of the two stars in the system (Percy 2007).

Around stars in single star systems the gravitational potential energy of the star is dependent on radial distance from the center of the star and is thus spherically symmetric. This changes for binary star systems. Since the two stars in a binary system are also orbiting closely around one another they each affect the gravitational potential energy spheres of the other and the rotating centrifugal force acting on the system must also be taken into account. These influences can be seen in Figure 4. Close to one of the stars the influence of the other is very small and the surfaces where the gravitational potential energy is constant remains spherical. But, as the distance from one star increases and comes closer to the second star the surfaces where the gravitational potential energy is constant begins to deform. Further deformation from a spherical shape is caused by contributions from the centrifugal force caused by the orbiting of the system about the center of mass.

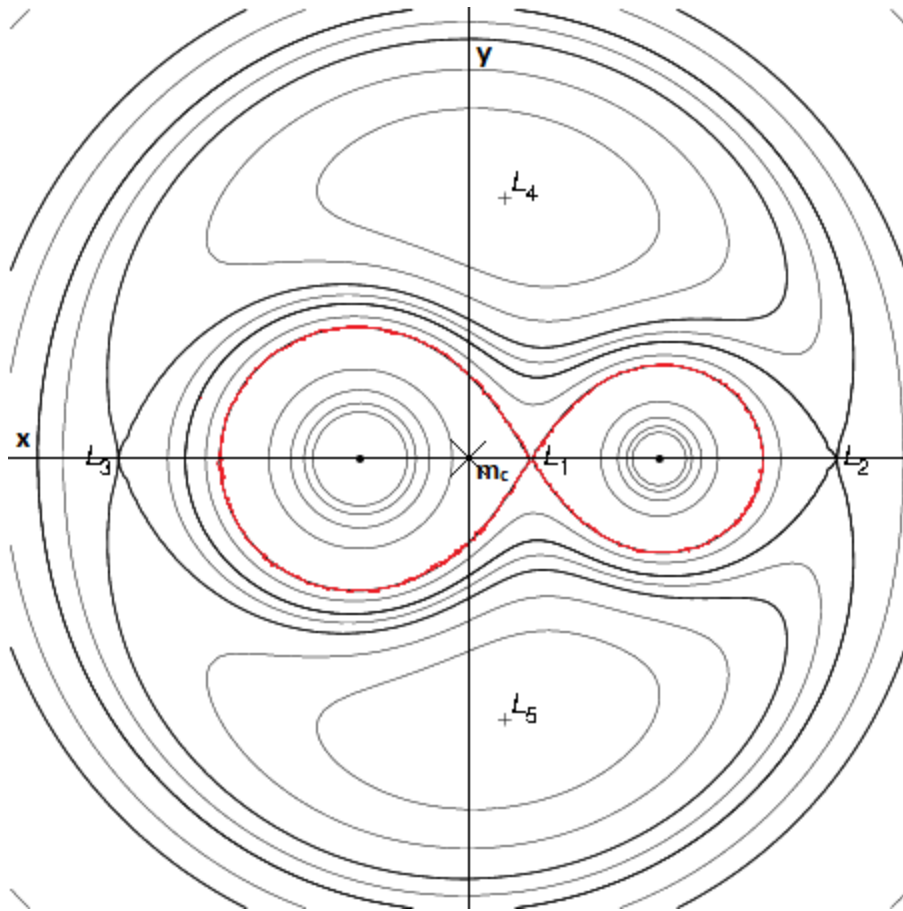


**Figure 4:** Display of equipotential surfaces about binary star systems. The highlighted red hourglass region defines the roche lobes for the system. The L1, L2, L3, L4, and L5 points are equipotential points for the system. The L1 point balances the gravitational and centrifugal potentials and connects the individual roche lobes for each star. L2 is a point of equipotential beyond the less massive star. L3 is a point of equipotential beyond the more massive star. These three points form a line through the center of mass of the system. The L4 and L5 points are points of equipotential at the points of equilateral triangles on either side of the line through the center of mass with the base of the triangle going from the center of one star to the center of the other. The reference frame for the system is centered on the center of mass. (Bhattacharyya 2009)

Eventually, the potential energy surfaces from each star meet at one point between them. This point is called the Lagrange 1 (L1) point. The surface of constant gravitational potential energy for this point forms an hourglass shape around the two stars. This has the benefit of breaking the potential energy surface into two distinct pieces. These pieces are the Roche lobes of the system, one for each star. Beyond this point the equipotential surfaces overlap each other.

The second method of classifying eclipsing binary star systems involves looking at how the stars in the system fill their individual Roche lobes. Over the lifetime of an individual star the stars surface can begin to expand. Over a long enough period of time the stars surface can expand to fill its entire Roche lobe. Examples of each type of eclipsing binary star system can be seen in Figure 5.

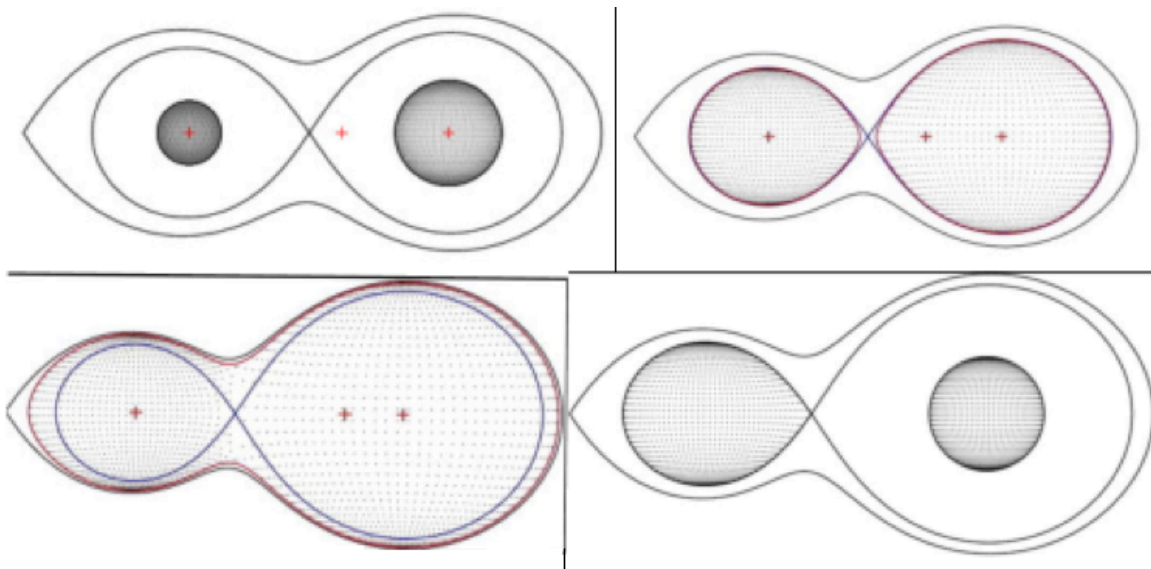


**Figure 5:** Examples of Roche lobe classification. The shaded areas in each panel define the surface of each star. Top Left: Detached binary system where neither star has filled its Roche lobe. Top Right: Close-contact binary system where both stars have filled their Roche lobes meeting at the L1 point and begun to equalize their temperatures through convection. Bottom Right: Semi-detached binary system where one star has filled its Roche lobe while the other hasn't. Bottom Left: Over-contact binary system where both stars have expanded beyond the bounds of their individual Roche lobes. Temperature equalization rate increases due to the sharing of a common convective envelope. The red lines in the Top-Right and Bottom-Left panels show the common convective envelope of the system ([http://www.eclipsingbinaries.prettyhill.org/about\\_ebs.htm](http://www.eclipsingbinaries.prettyhill.org/about_ebs.htm)).

If neither star is filling its Roche lobe the system is considered to be a detached system. If one of the stars in the system is filling its Roche lobe but the other star is not filling its Roche lobe then the system is called a semi-detached system. Also, since one of the stars has filled its Roche lobe up to the Lagrange 1 point, mass may be transferred from that star to the partner star that has not filled its Roche lobe through the L1 point. The

transfer of this mass can cause an accretion disk composed of stellar material to form around the star that has not filled its Roche lobe. It can also cause a hot spot to form either on the star itself or on the point of the accretion disk where the transfer material hits. This rising temperature of the accretion disk and the hot spot is caused by the impact as the matter falls from the L1 point to the surface of the star or the accretion disk around it. Beta Lyrae systems are commonly of this type. The third type of eclipsing binary system defined by how the stars fill their Roche lobes is one where both stars have filled their Roche lobes and are actually connected by sharing a common envelope. At this point, the two stars come into convective thermal contact and actually can begin to come to a common temperature. This is called a close-contact binary system and W Ursa Majoris systems are of this type. As the common envelope of the two stars continues to expand the system becomes known as an over-contact binary system. This increases the rate at which the two stars can reach thermal equilibrium. Examples of each of these situations can be seen in Figure 3.

### **1.3: Northern Sky Variability Survey**

The objects I observed were NSVS 5060083 and NSVS 5354761. Both of these systems were originally part of the Northern Sky Variability Survey (NSVS) (Wozniak, et al 2004). This was a large-area sky survey performed over the entire northern hemisphere and a small portion of the southern hemisphere northward of a declination of  $-38^\circ$ . The NSVS was a year-long survey conducted from April 1999 to March 2000 and recorded around 14 million objects of magnitudes ranging from 8 to 15.5. There were approximately 100-500 observations of each object taken over that year-long time period. The data used to generate the NSVS list came from the first generation Robotic Optical Transient Search

Experiment (ROTSE-I). The NSVS is a temporal record of the stellar objects in its observed area. Fortunately, other scientists have already looked at the very large list compiled by the NSVS and classified many of the objects within it.

Both of my objects were taken from a catalogue created from the NSVS and other objects by Hoffman, et al. (2008), specifically to find possible Algol and Beta Lyrae candidates. I chose my two targets specifically because further examination of them had yet to be performed. They had been determined to be variable by Hoffman, et al. (2008), but a closer examination of them, including observations at finer time resolutions and determination of stellar parameters had yet to be performed. Since the NSVS observations spanned over a year, the time resolution for these objects is on the order of days. The time between one observation and the next for the same object was several days. The NSVS was only able to get a few hundred images per object over the span of the year since there were so many objects to observe. This allows a view of what the light curve looks like and the ability to determine if the object is indeed variable or not. Since my objects vary on a time scale of less than a day, rather than several days, a finer time scale will give a much more precise look at the light curves of both of my objects by increasing the time resolution of the light curves.

## **Chapter 2: Observations**

All of my nights of observations were taken at two locations. The first is the Ball State University Observatory (BSUO) on the Ball State University Campus in Muncie Indiana located at  $40.1934^{\circ}$  N latitude and  $85.3864^{\circ}$  W longitude. The second location was the Southeastern Association for Research in Astronomy (SARA) 0.9 meter telescope located at the Kitt Peak National Observatory (KPNO) located 88 km west-southwest of

Tucson Arizona at  $31.9599^{\circ}$  N latitude and  $111.5997^{\circ}$  W longitude. SARA is a consortium of thirteen different universities that own and operate three observatories in three different countries. These telescopes include the SARA-KP telescope at Kitt Peak National Observatory in the United States, the SARA-CT telescope at Cerro Telolo in northern Chile, and the SARA-RM telescope at La Palma in the Canary Islands. I utilized the SARA-KP observatory. All observations were taken in three different filters Bessel B, V, and Cousins R.

At the BSUO site I used a 16" diameter Meade LX200 telescope equipped with an STXL-6303E CCD camera. The camera contains pixels  $9\ \mu\text{m}$  on a side and its chip length and width are 27.7 mm and 16.5 mm respectively. These combine to form a rectangular CCD of pixel dimensions of  $3072 \times 2048$  for a total of 6,291,456 pixels. The plate scale for this telescope is 0.457 arc-seconds per pixel. A computer program called The Sky 6 was used to control the telescope.

The 0.9-meter SARA telescope uses a CCD camera built by the company Astronomical Research Cameras Incorporated (ARC). The computer programs used to control both the dome and the computer at this site were built by Astronomical Consultants and Equipment Incorporated. The KPNO camera contained pixels  $13.5\ \mu\text{m}$  on a side and is a square CCD of pixel dimension of  $2048 \times 2048$  for a total of 4,194,304 pixels. The plate scale for this telescope is 28.3 arc-seconds per mm.

All images taken at these sites were binned  $2 \times 2$  to decrease file size. Squares of pixels with two pixels to a side were combined and read out as the equivalent of a single pixel. Adjustments were made to exposure times taken at each site based upon the telescope used and the particular seeing conditions of each night to optimize the signal to

noise ratio. Table 1 contains the location, standard date, and heliocentric julian date for my observations of NSVS 5060083. Table 2 contains the location, standard date, and heliocentric julian date for my observations of NSVS 5354761.

Location	Date	Julian Date
KPNO	4/5/15	2457117.5
BSUO	3/26/16	2457473.5
BSUO	4/12/16	3457490.5
BSUO	4/16/16	2457494.5
BSUO	5/29/16	2457537.5
KPNO	6/5/16	2457544.5

**Table 1:** Observational Data For NSVS 5060083. Telescope used for observations and the date and heliocentric julian date (HJD) of those observations for object NSVS 5060083.

Location	Date	Julian Date
BSUO	8/21/15	2457255.5
BSUO	8/24/15	2457258.5
BSUO	9/1/15	2457266.5
BSUO	9/2/15	2457267.5
BSUO	9/7/15	2457272.5
BSUO	4/12/16	2457490.5
BSUO	4/16/16	2457494.5
BSUO	4/17/16	2457495.5
BSUO	5/24/16	2457532.5
BSUO	5/29/16	2457537.5
BSUO	6/2/16	2457541.5
KPNO	6/5/16	2457544.5

**Table 2:** Observational Data for NSVS 5354761. Telescope used for observations and the date and heliocentric julian date (HJD) of those observations for object NSVS 5354761.

### Chapter 3: Data Reduction and Analysis

After observations were taken data reduction and analysis was performed. Data reduction was done using the Image Reduction and Analysis Facility (IRAF) software suite. Data reduction involved subtracting bias and dark field images and dividing out flat field images from the actual images of the target objects. Bias, dark, and flat field images were taken every night that images were taken of an object. When able these reduction images were also taken each morning as observations came to an end. Doing so gives us more images to combine together to get master bias, dark, and flat field images decreasing the error inherent in those master images.

The first step in IRAF was to combine the bias images into one master bias. Thirty to sixty bias images were taken each night of observation. Bias images are a zero second exposure of the CCD camera. This isolates the systematic offset from the chip itself and the electronics of the telescope. This offset is added to any image taken with the CCD and can be removed by subtracting out the master bias. Creating a master bias was done using the zerocombine command in the IRAF software suite. This created an average bias image that could then be subtracted from the other images. During the creation of this master bias pixels with values greater than three sigma from the mean are removed to reduce the effect of cosmic rays on the process.

The next step was to correct for the dark current generated by thermal fluctuations within the CCD chip itself. These effects are always present in a CCD. However, they can be greatly reduced by keeping the chip cool. The colder the chip is kept the less effect the thermal fluctuations have on the images taken with that chip. This is precisely what is done at the KPNO site. The chip is kept cooled to such a degree that the images taken there

did not need dark correction, as the influence of these thermal fluctuations was quite small. However, the BSUO site did not have the ability to keep its chip as cool as the chip at the KPNO so dark corrections had to be made with those images. The CCD at the KPNO site tends to be kept roughly twice as cold as the CCD at the BSUO site.

Three to six dark images were taken each night of observation. These images were taken at exposure times of six hundred seconds a piece. The exposure time is so long because the effect of the thermal fluctuations increases the longer images are exposed. I had to make sure that the dark images were exposed for much longer than any images I was going to get data from. The dark images were taken with the CCD shutter closed. This limits the counts detected to just those from the thermal fluctuations of the chip and the bias. During processing the bias in the image can be reduced by subtracting the master bias out of the dark images. The dark images are then combined together to find a median master dark image. A median is used to remove any effects caused by cosmic rays. Effects of cosmic rays can also be reduced by removing any pixel with values greater than three sigma from the mean. Since the master dark image has a much longer exposure time than the observational images involved, it is scaled to fit individual image exposure times before it is subtracted from those images. This scaling is done by the IRAF program itself and involves multiplying the master dark image by the ratio of the exposure times of the data images to the exposure time of the master dark image.

The next step in the process is to create a master flat field image for each filter. This is necessary since the sensitivity of the CCD chip is not uniform. Because of pixel by pixel variations in efficiency certain portions of the chip may be more sensitive to light than others. There are also going to be external effects that can affect the sensitivity of the CCD

over certain area. One of these effects is that caused by dust particles that have settled on or above each filter that can cast shadows on the CCD chip. These shadows on the chip lower the sensitivity of the chip in the area covered by the shadow. Another effect that can lower the efficiency of pixels in the CCD is an effect called vignetting. This occurs because the center of the CCD chip tends to be more illuminated than the edges of the chip (Berry and Burnell 2011).

In order to be able to find and remove these differences from the observational images the CCD chip must be evenly illuminated by light. To accomplish this we exposed the chip during twilight and, circumstances permitting, again at dawn. This results in between five and ten flat field images for each filter each night. With flat field exposures the number of counts for each pixel is more important than exposure time. The goal is to get a large enough number of counts so that it lies within the linear part of the CCD exposure. Each flat field image will have a different exposure time since the goal is to reach a number of counts halfway to the maximum necessary to saturate each pixel. The IRAF software is again able to scale the flat field images. But this time it scales each pixel to an average flat field value found in the center of the master flat for each filter by creating a ratio of each pixel to that average flat value. In order to combine the flat images into a master flat for each filter the command `flatcombine` was used. This command averages all the flats for each individual filter together create a master flat that can be divided out of the observational images for that particular filter. Before combining the individual flat field images the master dark and master bias are subtracted out of each flat field image.

So now for each individual observational image we can use the `ccdproc` command from IRAF to subtract out the bias and dark frames and divide out the flat field images.

This gives us a much better image upon which to perform photometry than the initial raw image. The systematic offset from the electronics is removed by subtracting out the average bias, the thermal currents of the system are removed by subtracting out the median master dark, and pixel by pixel variation is reduced, artificial background objects caused by dust were removed, and vignetting effects were reduced by dividing out the master flats. With the removal of artificial background objects, caused mainly by dust settling on the filters, the background of each image is much cleaner allowing much more accurate aperture photometry to be performed. This concludes the image reduction process and we can move on to the analysis of the images.

After reducing the data but before continuing on to the photometric analysis of our images there is one more step to perform. Our telescope records current date and time in a Julian Date (JD) format. Unfortunately, we want this to be converted to a Heliocentric Julian Date (HJD) format. The heliocentric Julian date format takes into account the position of earth in its orbit around the sun and moves the frame of reference from that of earth to the center of the sun. This allows me to combine multiple observations of my objects since they now all share the same reference location. Fortunately for us IRAF has a simple way to correct for this. It can determine the heliocentric Julian date as long as we also have an epoch defined in the header notation. This was not naturally included in the header information for our images but was added manually by creating a line in the header called EPOCH 2000.

Now that the images have been reduced we can begin to actually perform photometric analysis on them. I chose to use the software suite Astronomical Image Processing for Windows (AIP4WIN) (Berry and Burnell 2011) for my photometric analysis.

This program uses aperture photometry to determine the differential flux of a target object at a certain time versus a comparison star. By combining this with multiple exposures of the same object over time we can see if and how the objects flux varies over time. This also allows us to create a light curve for our object, which after further analysis will give us the period of the object.

How aperture photometry works is a series of three concentric circles, or apertures, are placed around the object in question. The innermost aperture ring encloses the object we are interested in. This ring measures the flux of that object as well as a small amount of leftover sky background. The program ignores the area between the first aperture and the second aperture. This allows a little leeway for the program in case light from the object goes beyond the bounds of the first aperture ring. The area between the second aperture ring and the third aperture ring determines the flux value of the sky background of the image. In order to find the value of the flux within the first aperture ring the program subtracts the average flux value of the sky background from the flux value within the first aperture normalized relative to the area of the aperture used.

However, with differential aperture photometry we not only have apertures around our target object we also have them around two other objects. One of these is called our comparison star and the second is called our check star. By performing aperture photometry on the comparison star as well as our object of interest we can now have flux values for two stellar objects in our field of view. This allows us to create a flux differential between our comparison star and our object of interest. If this differential changes over time then our object is a variable star. By graphing the flux differential over time we can create a light curve for our object of interest.

It is very important to note that this differential flux can only be used if our comparison star does not also vary over time. If it did vary over time then our flux differential would be meaningless. This is where our check star comes into play. By performing aperture photometry across our check star as well, we can create another flux differential between our comparison star and our check star. If neither of these stars are variable then the light curve we can generate from this should be a nearly straight line. If this is not what is seen then different comparison and check stars need to be chosen until it is. Otherwise, the variability of the target star would be lost within the variability of our comparison star. Figure 6 contains an image of the star field for NSVS 5354761 with the target, comparison star, and check star clearly marked. Table 4 contains the designation, location in RA and Declination, and epoch for each of these star systems.

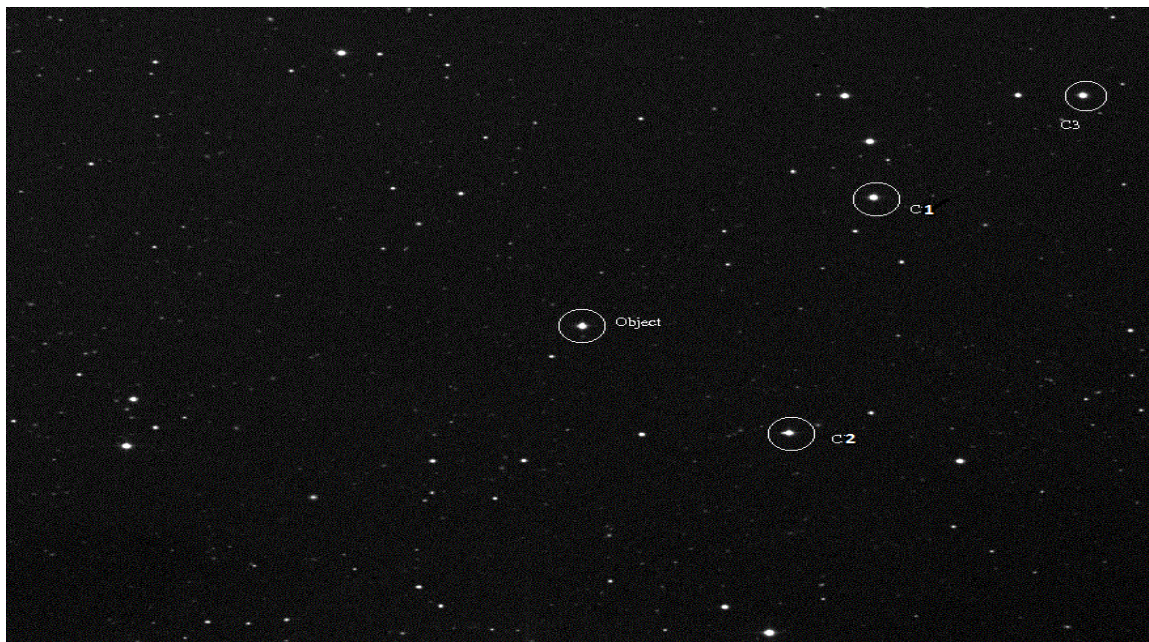


**Figure 6:** Star field for NSVS 5060083. This is a POSS2/UKSTU red image ([stdatu.stsci.edu/cgi-bin/dss\\_form](http://stdatu.stsci.edu/cgi-bin/dss_form)). Marked on the image are the location of the target object, the comparison star (C1), the check star (C2), and a second check star (C3). C1 is the comparison star used by AIP4WIN to measure the difference in flux for the target system over time. It is required to be a non-variable star system. C2 is the check star used to confirm that C1 is indeed a non-variable star system. C3 was used to help determine the magnitude of target star during the calculation of the (B-V) value for the target since neither C1 nor C2 had known B or V values. The image is 22 arcminutes high by 24 arcminutes wide.

Object	Designation	RA	DEC	Epoch
Target	NSVS 5060083	13° 20' 57.67"	+47° 29' 30.24"	J2000
C1	GSC 3460:2240	13° 21' 01"	+47° 28' 31"	J2000
C2	GSC 3460:2250	13° 21' 14"	+47° 20' 28"	J2000
C3	LP 172-75	13° 19' 54.03"	+47° 37' 02.8"	J2000

**Table 3:** Celestial coordinates and designations of target and comparison stars for NSVS 5060083 star field.

Figure 7 contains an image of the star field for NSVS 5354761 with the target, comparison star, and check star clearly marked. Table 4 contains the designation, location in RA and Declination, and epoch for each of these star systems.

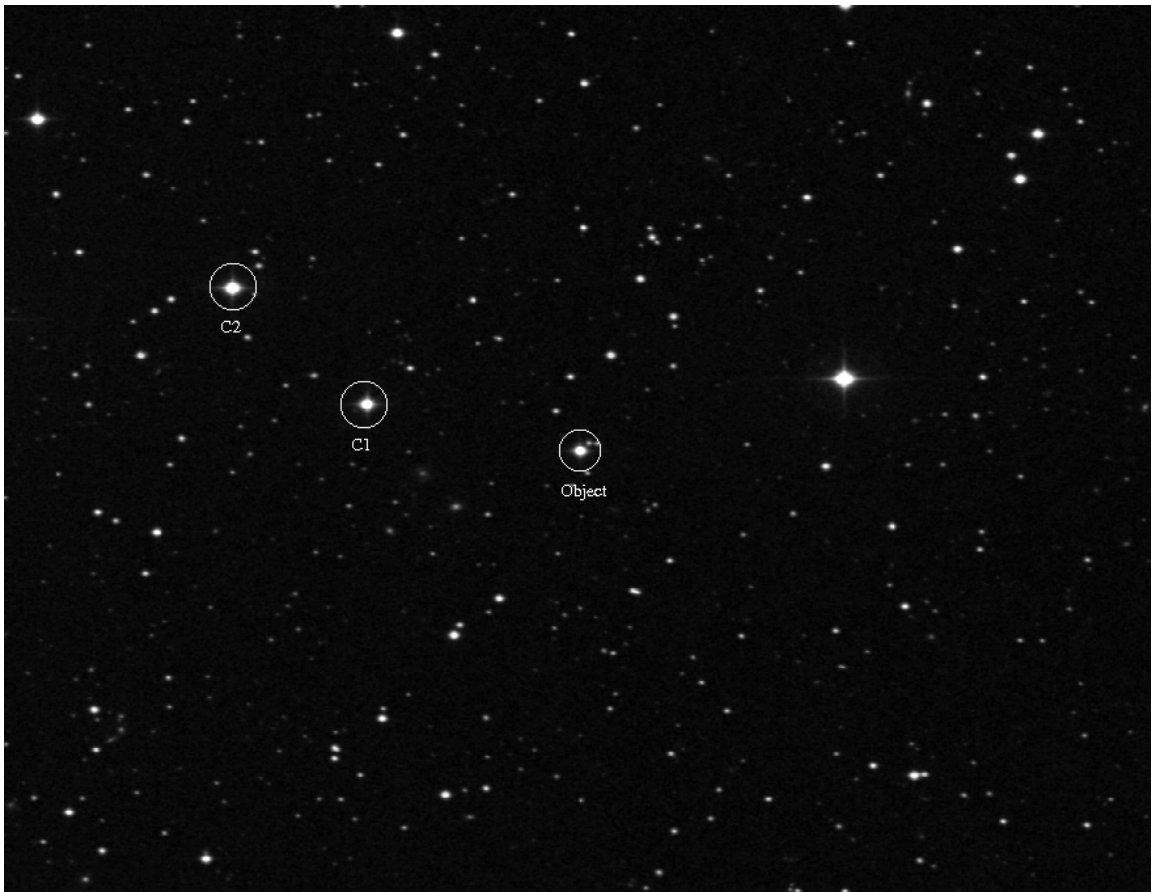


**Figure 7:** Star field for NSVS 5354761. This is a POSS2/UKSTU red image (stdata.stsci.edu/cgi-bin/dss\_form). Marked on the image are the location of the target object, the comparison star (C1), and the check star (C2). C1 is the comparison star used by AIP4WIN to measure the difference in flux for the target system over time. It is required to be a non-variable star system. C2 is the check star used to confirm that C1 is indeed a non-variable star system. The image is 15 arcminutes high by 15 arcminutes wide.

Object	Designation	RA	DEC	Epoch
Target	NSVS 5354761	17° 46' 15.04"	+45° 23' 31.79"	J2000
C1	GSC 3510:1406	17° 46' 58"	+45° 24' 23"	J2000
C2	GSC 3510:1462	17° 47' 08"	+45° 26' 20"	J2000

**Table 4:** Celestial coordinates and designations of target and comparison stars for NSVS 5354761 star field.

Now that our images have been reduced and we have generated our light curves using AIP4WIN the next step is to determine the period of variability of our objects of interest. There can be several difficulties in doing this. The most common complication is that the period of the object may be longer than can be seen in one nights worth of observation and thus longer than can be seen on one nights light curve. Also, seeing conditions may limit the amount of observations that can be accomplished in one night. For example, clouds may begin to cover the sky partway through the night preventing further observations. As a result, instead of having one continuous light curve for an object over one night we may have several smaller portions of the total light curve over several nights of observation.

This is further complicated by the fact that the flux of the object continues to vary over the entire day. This is combined with the fact that making observations every single night is nearly impossible due to both seeing and weather conditions as well as the fact that the object may not be observable the entire year. As a result, several nights of observation might overlap the same position on the light curve of a target object. This is precisely the problem I ran into when looking for a complete light curve for NSVS 5354761. This is why there are so many observations for that object as opposed to NSVS 5060083.

In order to solve these problems something that is called a folded light curve must be created. To create a folded light curve all the light curves generated for each night are

taken and “folded” around a series of periods until one particular period is found that is the best fit for all the individual light curves. This takes all the individual light curves from each night and places them in one continuous light curve. To do this the PERANZO: Light Curve and Period Analysis Software suite (CBA Belgium Observatory 2011) is used. The PERANZO program takes the individual pieces of the light curve from each night of observation and attempts to combine them into one continuous light curve over a range of periods until it finds the ideal one.

While PERANZO has several ways to accomplish this I chose to produce periodograms using the Analysis of Variance (ANOVA) method with twelve harmonics. A periodogram calculates the significance of different periods in a series of time-based data in order to identify the most likely period for the entire series. This uses periodic orthogonal polynomials to fit a series of possible periods to the data. It then uses statistics to determine what the best period is to use for the data (Schwarzenberg-Czerny 1996). The program allows us to define a range of possible periods. This limits the program to examining the statistical likelihood of periods within that range. Since my objects were included in the Hoffman, et al. (2008) catalog I already had preliminary periods to use in PERANZO. This allowed me to limit the period search range the program used and to increase the sensitivity of the program over that range to more precisely pinpoint the actual period. Examples of the periodograms and light curves generated by PERANZO can be seen in Figures 8, 9, and 10.

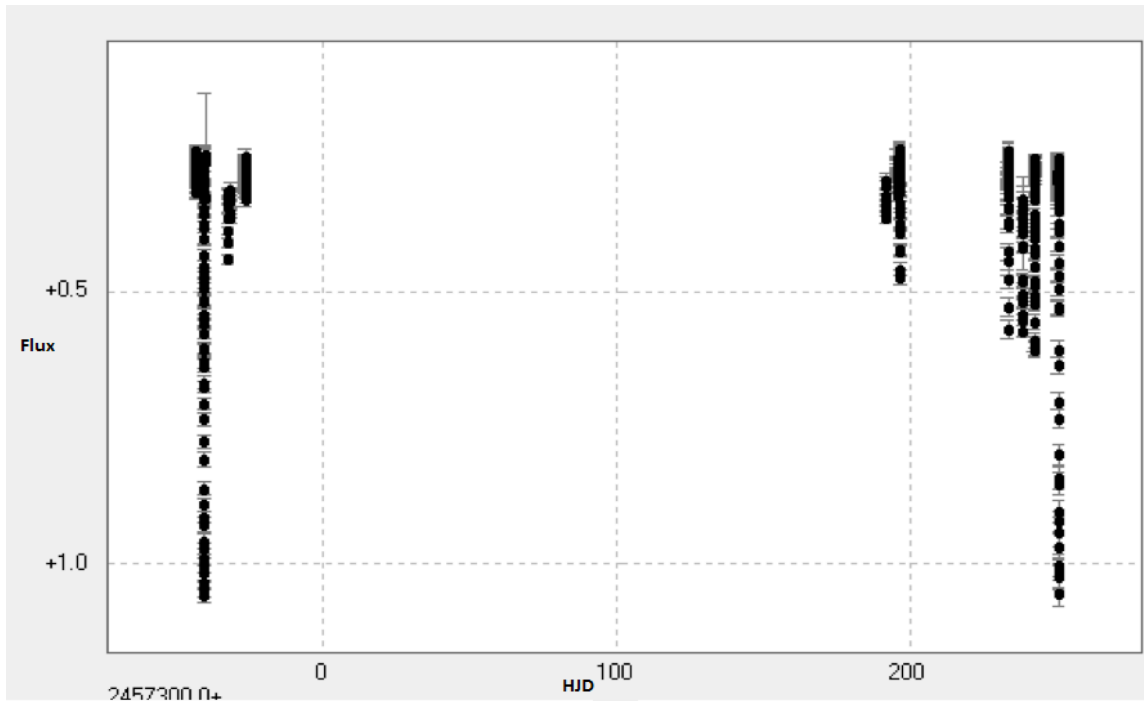


**Figure 8:** Observational data when inserted into PERANZO. Several nights worth of observational data can be seen here. Each nights data appears as a series of flux values in a vertical line because of the timescale of the graph. Some of the nights are separated by several months. This highlights one of the problems that PERANZO is used to solve. Combining these disparate groups of data into one continuous light curve.

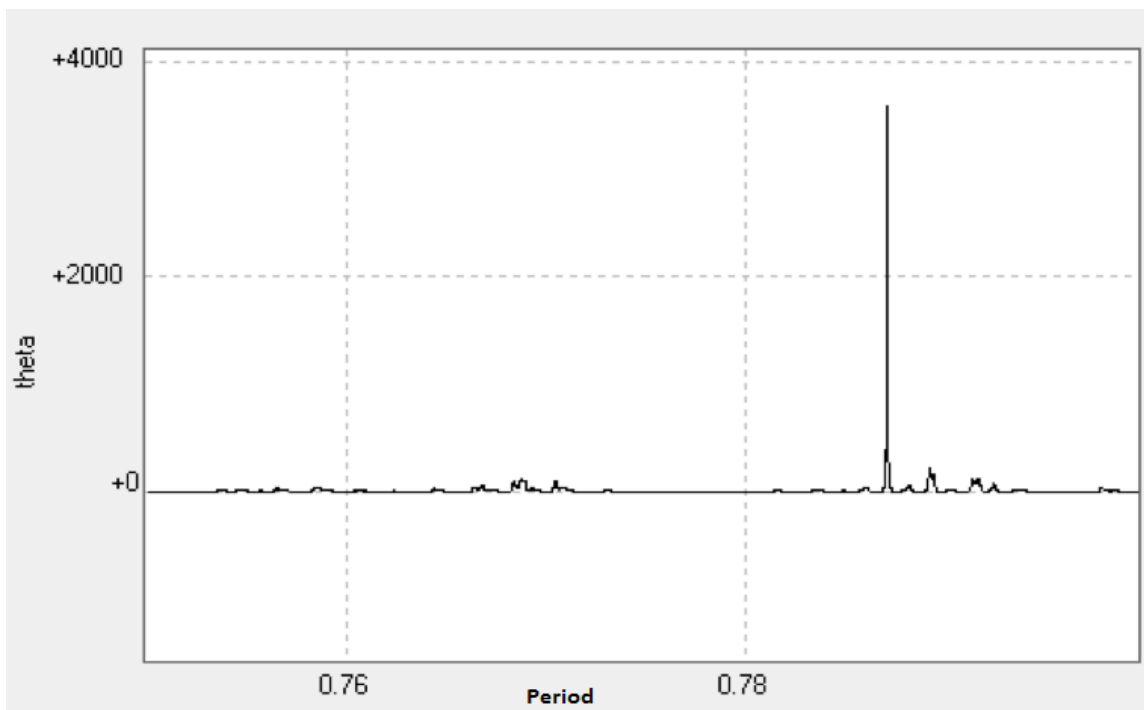


**Figure 9:** Periodogram example from PERANZO for NSVS 5354761. This figure shows a completed periodogram for NSVS 5354761 in the B filter. The theta value all the y-axis is a measurement of how likely a particular period is to be the actual period of the system. The greater the theta value the more likely that period is to be the correct one. The period is measured in portion of a day.

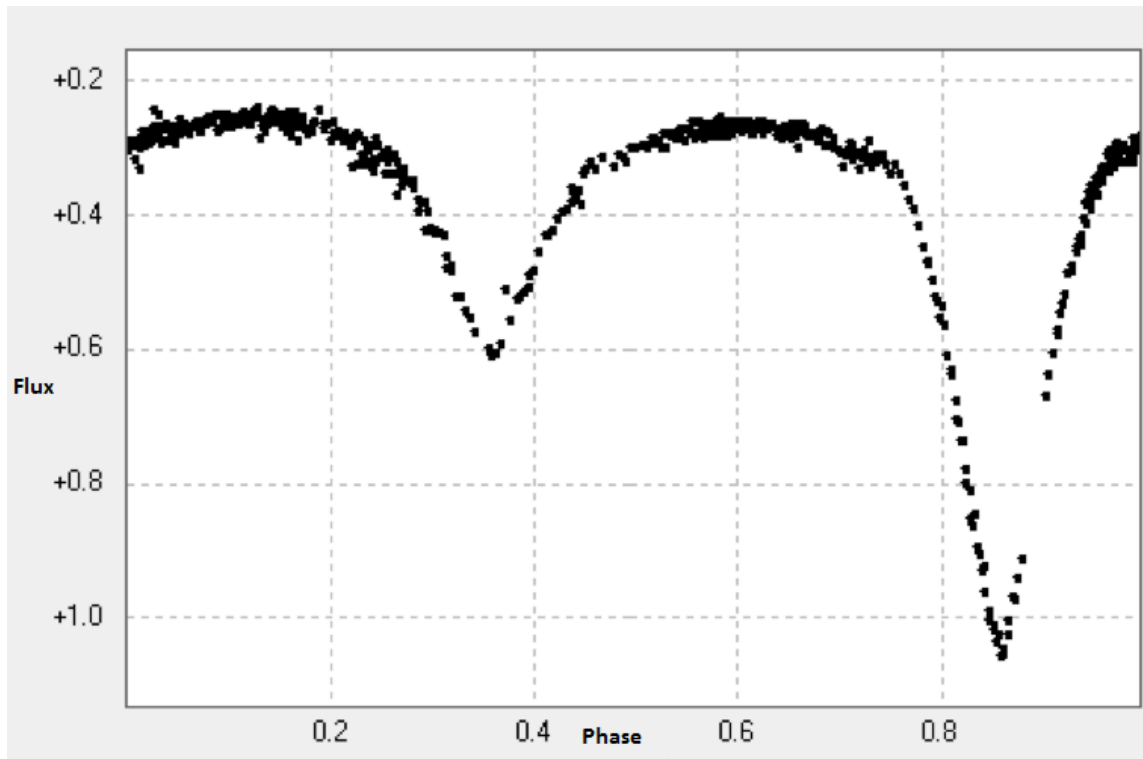


**Figure 10:** Example of a PERANZO constructed light curve. Light curve generated by PERANZO for NSVS 5354761 in the B filter. This is exactly the same data as in Figure 8 but has now been matched to the period found in Figure 9 in order to provide a single continuous light curve..

The PERANZO program chooses the period with the greatest statistical likelihood. This is not always the period that generates a complete and clean light curve. In particular for NSVS 5454761 PERANZO kept supplying a period that was obviously incorrect as the light curve it generated using that period was neither clean nor continuous. Some of the nights appeared disjointed and separated from the main body of the folded light curve. Fortunately, PERANZO allows you to manually manipulate the period using a graphical interface while simultaneously changing the light curve it displays as you do so. This allowed me to find a period for the variability of NSVS 5354761 that did result in a clean and contiguous light curve. Which was actually not entirely that far off from the value that PERANZO found more statistically likely.

It was at this point in my analysis that I ran into one additional problem with the observations. Partway through 2016 the filters for the BSUO 16-inch telescope were changed. It was decided that replacement of the B and V filters for the telescope was advisable. As a result images taken with the new filter set showed an offset from the original filter set. Images taken using the aged filter were found to have less flux than those taken after when both sets of data were placed into PERANZO. While the differential light curves were very similar they were offset vertically by a constant amount. Of course this amount was also different for each filter. It was thus necessary to correct for this discrepancy in order to use data taken before the replacement with data taken after the replacement. So the older data need to be adjusted to bring it in line with the newer observational data.

The trouble here was to determine precisely where on the light curve the pieces from before the replacement belonged when compared to after the replacement. One of the nights of observation from before the replacement contained data that included the primary eclipse of the object. I also had a night of observations for this primary eclipse from after the replacement. By shifting the primary eclipse data from before the replacement to match that from after the replacement I was able to determine the amount of offset between the two sets of data. I could then perform the same offset on all other sets of data from before the replacement and correct them as well. For the B filter data a flux value of 0.11 was added to each observation. For the V filter data a flux value of 0.06 was added to each observation. This made the period fitting in PERANZO much easier and gave a much more precise period fit. It was not necessary to do this for my observations of NSVS 5060083 as all those observations were done using the old filters.

## Chapter 4: Modeling With PHOEBE

After finding the period of my objects of interest with the PERANZO program it was time to start modeling the systems. In order to do this I imported the light curve data into the Physics of Eclipsing Binaries (PHOEBE) program (Prsa 2011). PHOEBE is a GUI interface designed to aid in the modeling of stellar systems using the Wilson-Devinney code (Wilson and Devinney 1971).

PHOEBE relies on many different parameters to create a model of the light curve of a system. It then takes the light curve that it generates from these properties and overlays it onto the light curve generated from experimental observations. It can do this using very few initial parameters. The only ones necessary to begin the process are an epoch time taken to be the time of minimum of the primary eclipse of the object, the period of variability of the object, and the temperature of the primary star in the binary star system. Other parameters of the system such as orbital inclination, secondary star temperature, and the mass ratio of the system can be extracted using the Wilson-Devinney code after the modeling process is complete.

During the modeling process the set parameters are not changed. However, over the course of the modeling PHOEBE automatically adjusts several other parameters in order to make the model match the observed data. I began by choosing the luminosity levels for the primary star. Once these had settled to a value a refused to change anymore I began to add in other parameter. Each time I added a new parameter PHOEBE would adjust the model to reflect the fact that that parameter was now free to change. Eventually, the list of parameters included not just the primary star luminosity levels but also the

effective temperature of the secondary star, the secondary stars surface potential, the mass ratio of the system, and the inclination of the system.

The period used came straight from the PERANZO fits. The time of minimum is actually the time at the center of the primary eclipse of the system. This was found using a program (Robert Berrington, Private Communication, 2016) based on techniques provided by Kwee and van Woerden (1956). In order to find the temperature of the primary star of the system we used another program (Robert Berrington, Private Communication, 2016). This program provides instrumental (B-V) values using data entered by the user. It does this over the entire span of the light curve but since we are only interested in the temperature of the primary star we look at the (B-V) when the primary star eclipses the secondary star, i.e. the secondary eclipse. We look at this particular value because this is when the majority of the flux comes from the primary star whose temperature we are ultimately looking for. This is at a phase of 0.5 for our light curve since the center of the primary eclipse begins our light curve and is at a phase of 0. Figures 11 and 12 show the (B-V) graphs created for my objects NSVS 5060083 and NSVS 5354761 respectively.

Once we have the (B-V) value for this position we must now account for interstellar extinction effects. To do this we used the NASA/IPAC Extragalactic Database (NED) Coordinate and Extinction Calculator, which is based upon the work of Schlafay and Finkbeiner (2011). We then subtract this interstellar extinction from the (B-V) values we found previously to determine our final (B-V). We can then determine the temperature value of the star using resources ([www.uni.edu/morgans/stars/b\\_v.html](http://www.uni.edu/morgans/stars/b_v.html)) based on the work of Flower (1996) and Torres (2010).

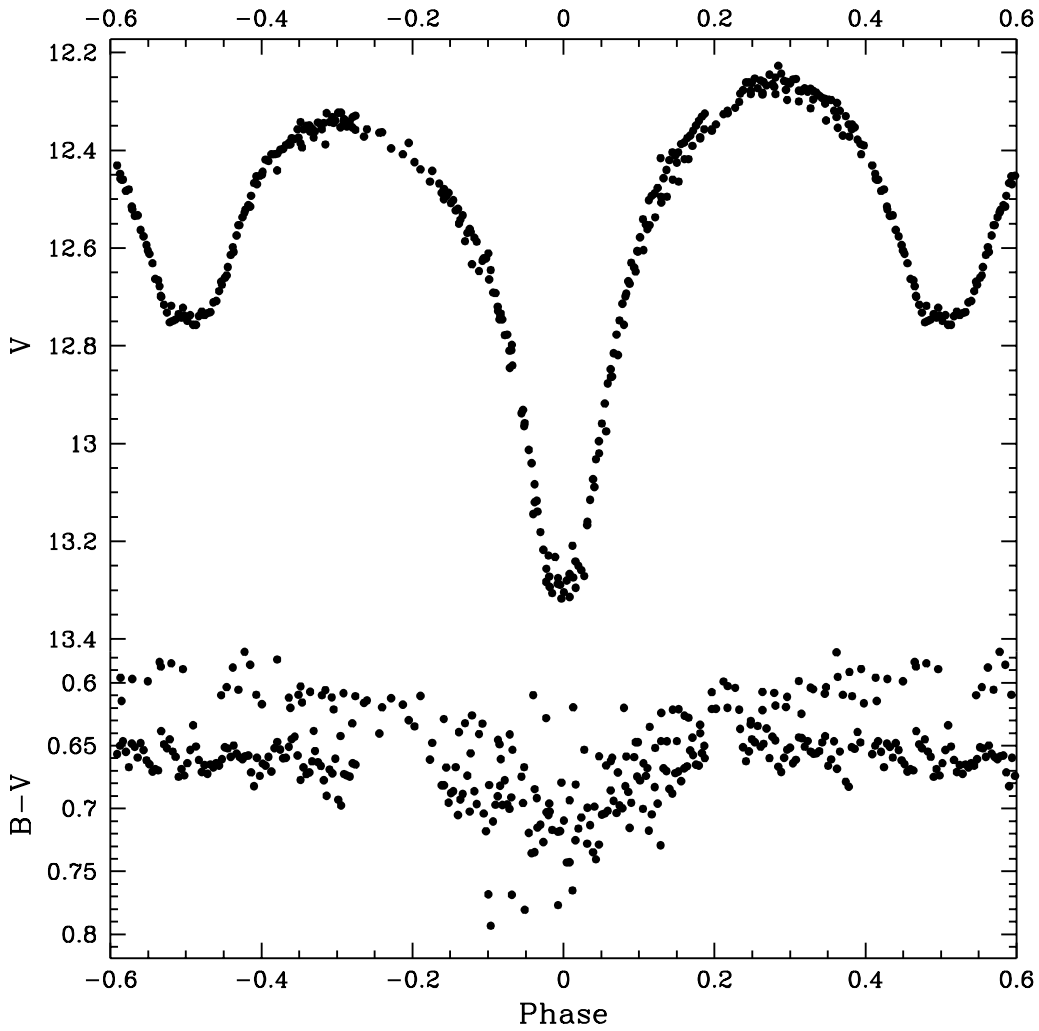


**Figure 11:** (B-V) Graph for NSVS 5060083. Only the V light curve is shown here with magnitude shown on the y-axis and the phase along the x-axis. The B curve is not shown as it is beyond the bounds of the figure. At the bottom of the figure is the (B-V) at each phase of the light curve. To find the temperature of the primary star the (B-V) value at a phase of 0.5 is determined.

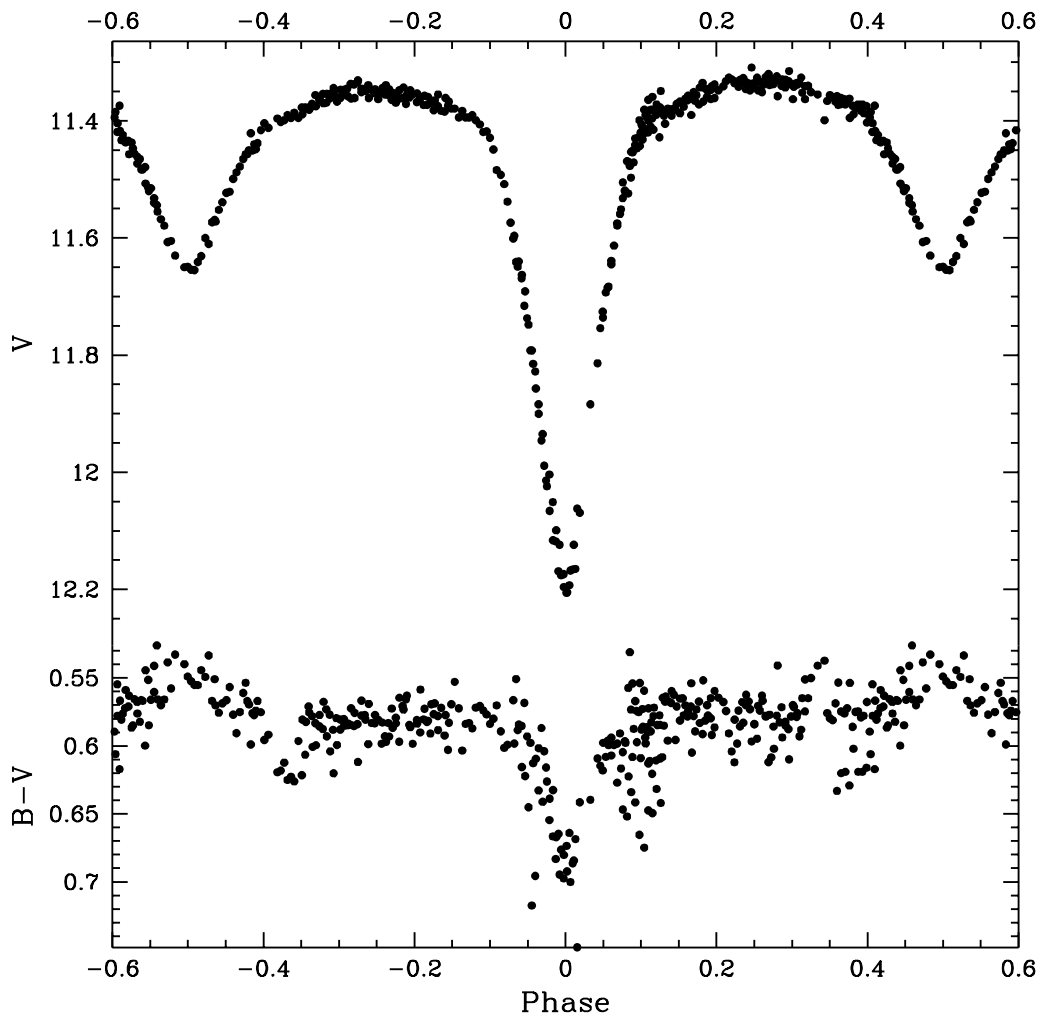


**Figure 12:** (B-V) Graph for NSVS 5354761. Only the V light curve is shown here with magnitude shown on the y-axis and the phase along the x-axis. The B curve is not shown as it is beyond the bounds of the figure. At the bottom of the figure is the (B-V) at each phase of the light curve. To find the temperature of the primary star the (B-V) value at a phase of 0.5 is determined.

It is important to note that the data used to develop the (B-V) curves cannot be the relative fluxes that were used previously when creating the light curves. These relative fluxes must be corrected to the magnitude value of the object of interest over time. In order to make this correction it is a matter of using secondary standard stars to find the magnitude values for the object of interest. This is much easier to do this when the magnitude of the comparison star is known in each filter since we already have the difference between those stars and our objects of interest. This was the case with my NSVS 5354761 object. However, with regards to my NSVS 5060083 object the magnitudes in each filter of the comparison star I used were unknown and there were no known magnitude stars within the field of view that were usable for our purposes.

This problem was solved by moving the telescope to center more on the comparison star. This changed the field of view of the telescope to include a star whose magnitude values were known which is labeled as C3 in Figure 6. By performing differential aperture photometry between my comparison star and this known magnitude star I was able to determine the magnitude of my comparison star in each filter. I was then able to use this calculated magnitude to find the magnitude of NSVS 5060083 over time and thus to determine its (B-V) value and the temperature of its primary star.

## **Chapter 5: Results**

### **5.1 NSVS 5354761**

The analysis for this object was pretty straightforward once data collection was complete. The PHOEBE created light curve matches solidly with the observed light curve except in one respect. There is a portion of the light curve during the climb out of the secondary eclipse where the light curve dips again slightly. The cause of this effect is

unknown. It does appear to remain consistent over several nights of observation but more data is needed to confirm this.

The light curve for this system was modeled several ways but the best model by far was using a detached system. As can be seen from the curve in Figures 13, 15, and 17 the light curves change continuously and the depths of the primary and secondary eclipses are different. This light curve marks the system as a Beta Lyrae system even though the model used in PHOEBE implies a detached system. The designations and celestial coordinates of the comparison and check stars for this system can be seen in Table 4. The secondary standard star used to determine the (B-V) value for this system was the C1 star on that table. The (B-V) for the system was determined to be 0.58 while interstellar extinction was determined to be 0.02 leading to an intrinsic (B-V) value of 0.56. This translates to a primary star temperature of approximately 6044 K. The period of the system as determined by PERANZO is  $0.787155 \pm 0.000006$  days. The orbital inclination determined from PHOEBE was  $78.41 \pm 0.07$  degrees with a mass ratio of  $1.2693 \pm 0.0094$  and a secondary component temperature of  $4976 \pm 6.7$  degrees K. The average time of minimum for the system over all three filters was  $2457259.634606 \pm 0.000148$ . Figures 13-18 are the light curves and their residuals for all three filters, Bessel B and V and Cousins R. Figure 19 is a 3D representation of the two stars at four positions in their orbits around one another. These four positions are at an orbital phase of 0.25, 0.5, and 0.75 of its period. As can be seen on this 3D representation there is a slight deformation of the larger star towards the L1 point. It has expanded slightly within its Roche lobe.

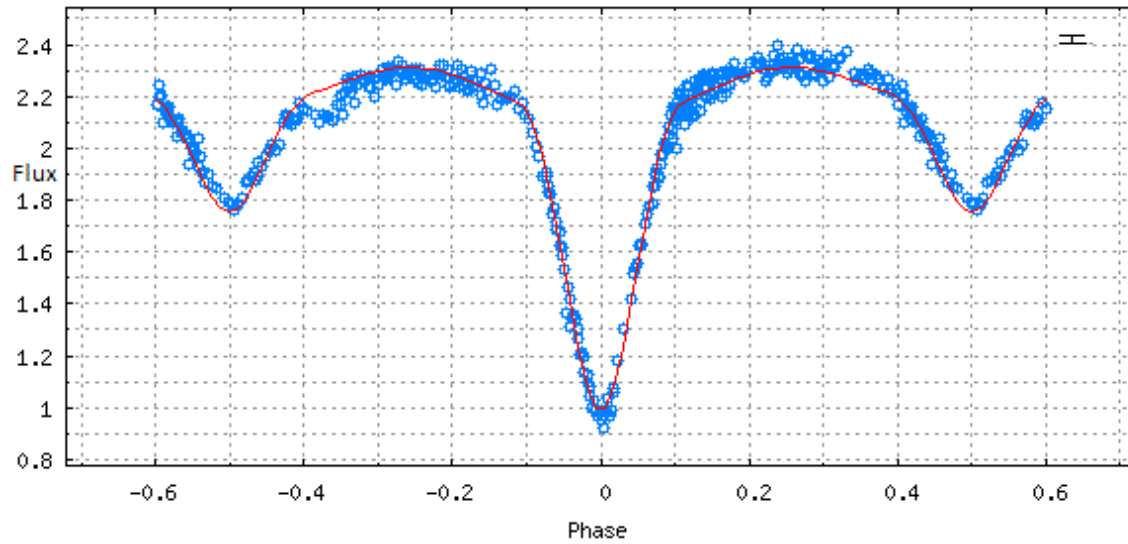


**Figure 13:** Folded light curve in Johnson B filter for NSVS 5354761. Plot of observational data (hollow circles) overlaid with the best-fitting model light curve from PHOEBE (solid curve). Error bars are omitted for clarity but a typical error bar can be seen in the upper right hand corner with a value of  $\pm 0.02$ .

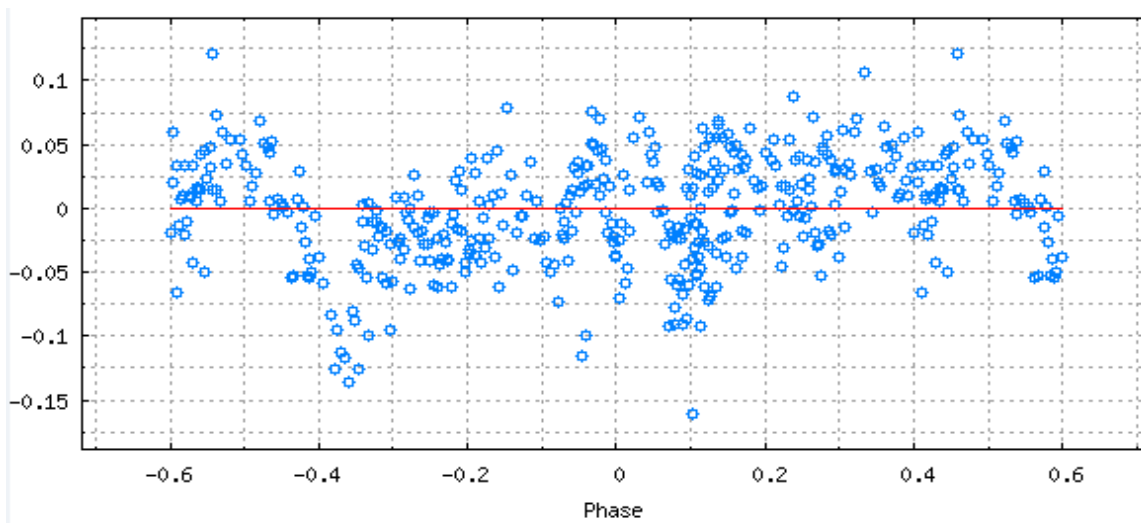


**Figure 14:** Residuals for folded light curve in Johnson B filter. Plot of the difference between the projected light curve generated from PHOEBE (solid line) and the observational data (hollow circles).

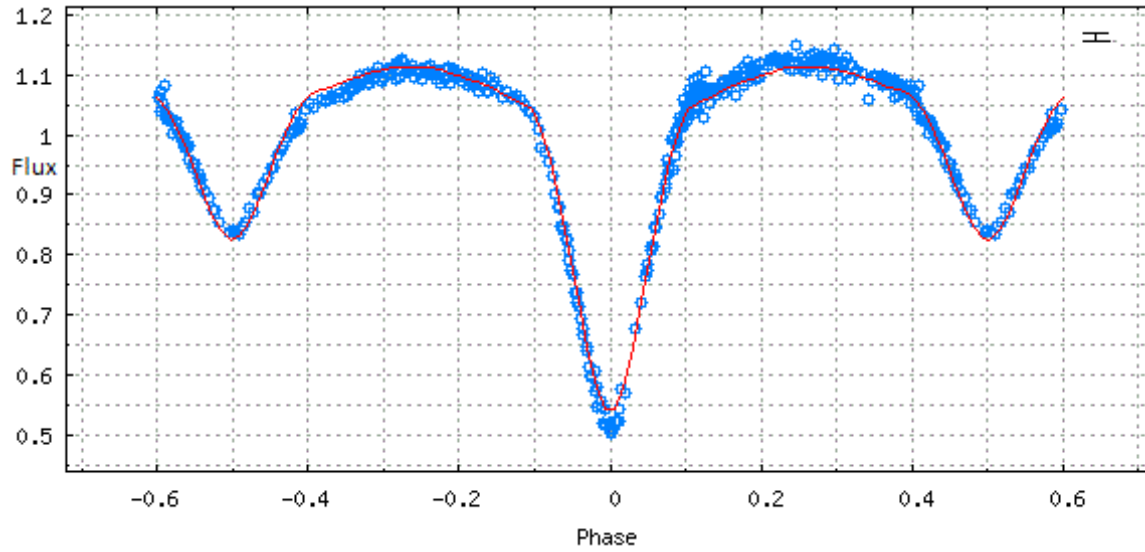


**Figure 15:** Folded light curve in Johnson V filter for NSVS 5354761. Plot of observational data (hollow circles) overlaid with the best-fitting model light curve from PHOEBE (solid curve). Error bars are omitted for clarity but a typical error bar can be seen in the upper right hand corner with a value of  $\pm 0.02$ .

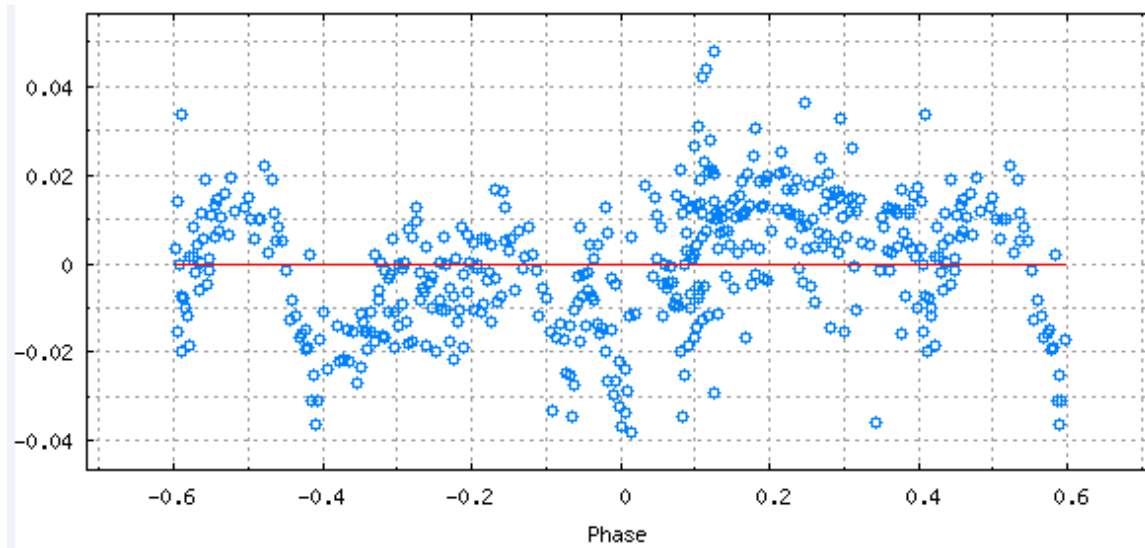


**Figure 16:** Residuals for folded light curve in Johnson V filter. Plot of the difference between the projected light curve generated from PHOEBE (solid line) and the observational data (hollow circles).

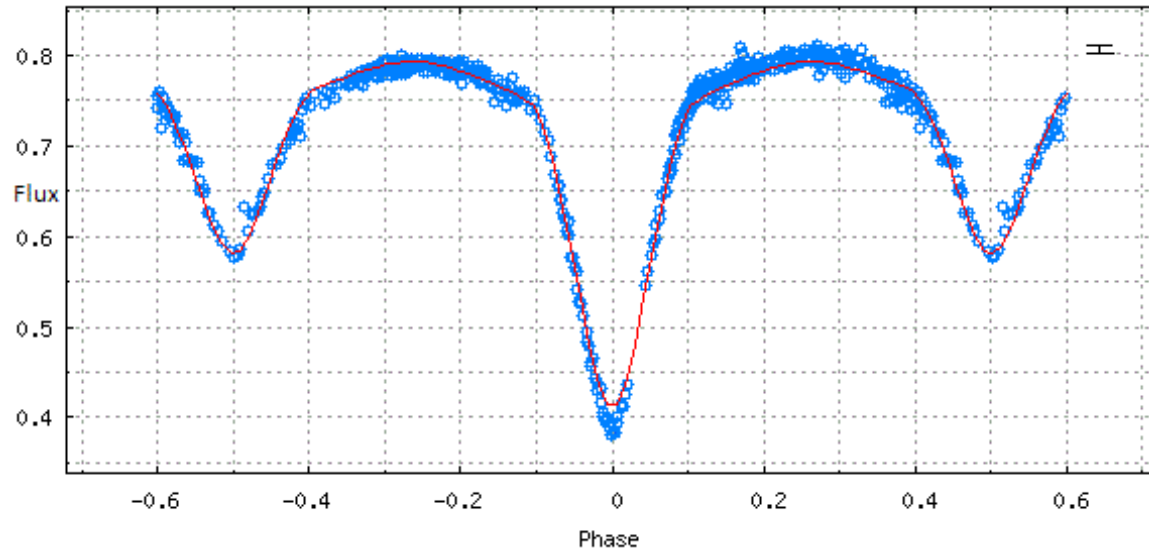


**Figure 17:** Folded light curve in Cousins R filter for NSVS 5354761. Plot of observational data (hollow circles) overlaid with the best-fitting model light curve from PHOEBE (solid curve). Error bars are omitted for clarity but a typical error bar can be seen in the upper right hand corner with a value of  $\pm 0.02$ .

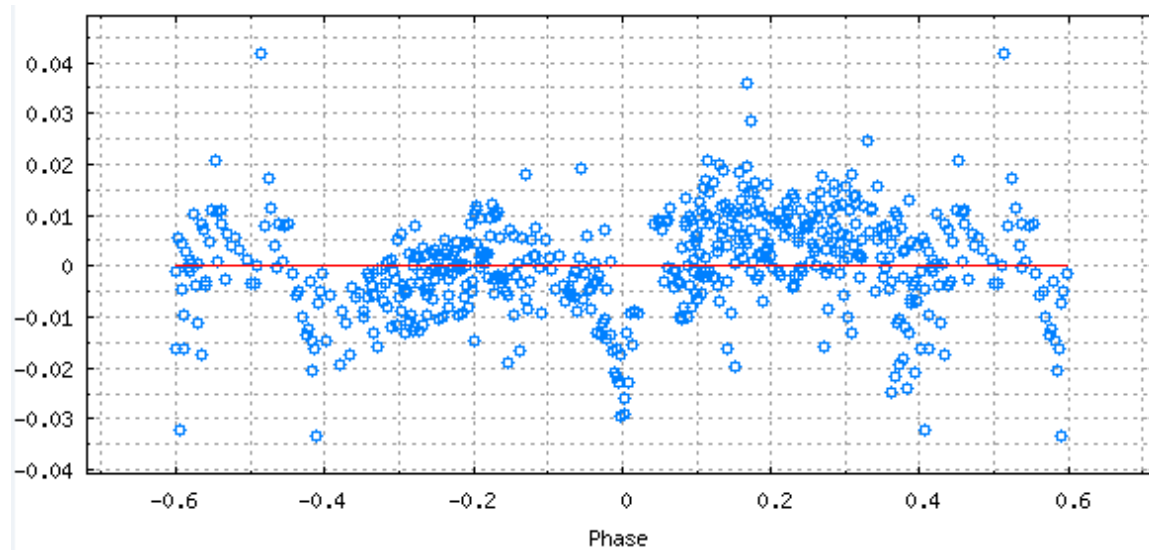


**Figure 18:** Residuals for folded light curve in Cousins R filter. Plot of the difference between the projected light curve generated from PHOEBE (solid line) and the observational data (hollow circles).

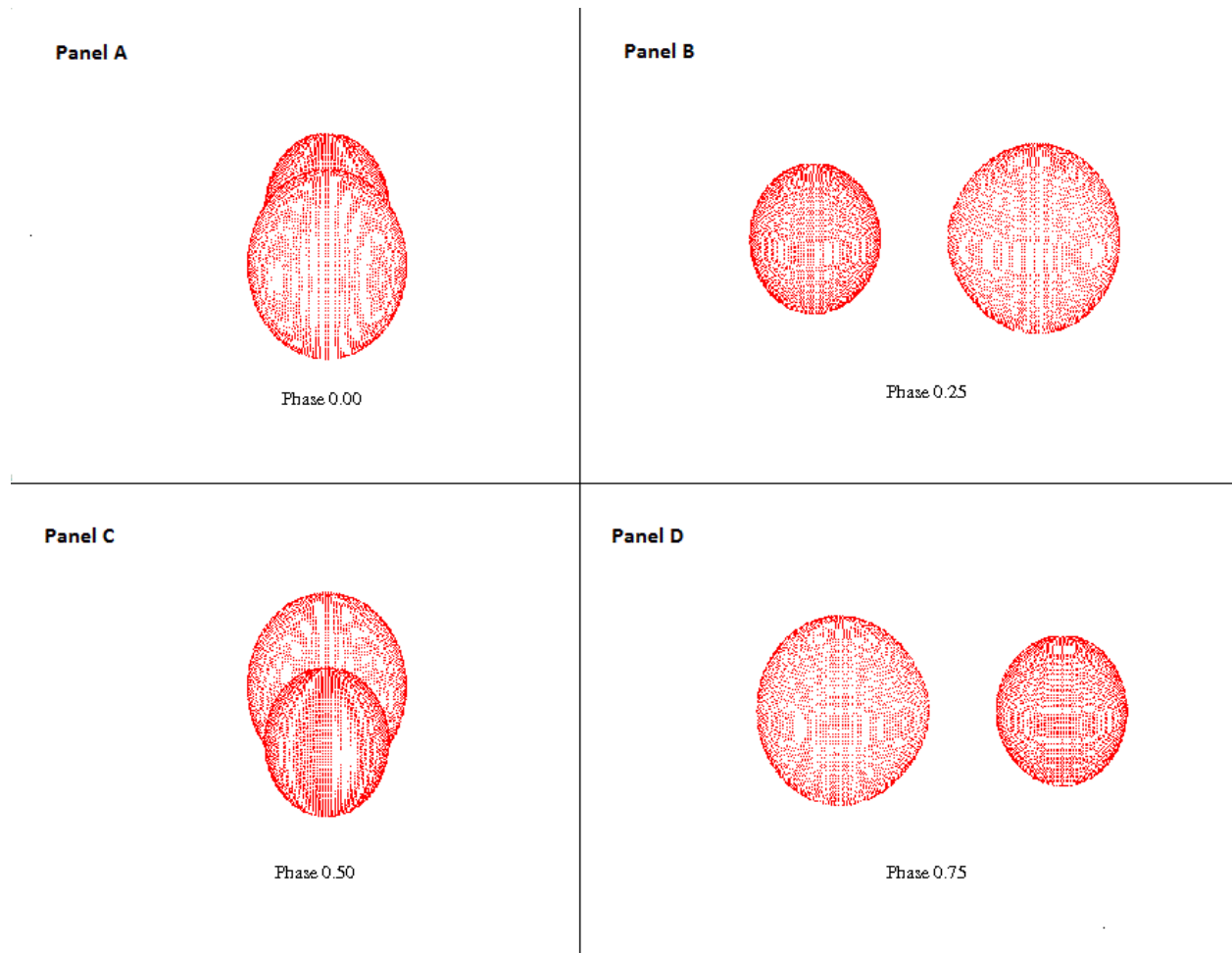


**Figure 19:** Three Dimensional Models of NSVS 5354761. Beginning at top left with a representation of the primary eclipse (Phase 0.0) at Panel A and continuing to display the binary system at orbital phases of 0.25, 0.5 (the secondary eclipse), and 0.75 at Panels B, C, and D respectively.

## 5.2 NSVS 5060083

The analysis for NSVS 5060083 was more complicated than that for NSVS 5354761. The major complication for the system was that it was very difficult to determine what type of stellar system it was and thus which model to use to analyze it. Throughout the analysis process the secondary star would keep deforming and overlap with the primary star in an erroneous manner. This effect can be seen in Figure 20. The issue was further exasperated when the overcontact model was attempted. This model was unable to match the observed

light curve. Ultimately a semi-detached model was chosen for the analysis. This was chosen since it resolved the previous error in the 3d modeling while also matching the observed light curve.

As can be seen from the curves in Figures 21, 23, and 25 the light curve for NSVS 5060083 also changes continuously and the depths of the primary and secondary eclipses are different. This marks the system as a semi-detached Beta Lyrae system. The designations and locations for the comparison and check stars for this system can be seen in Table 3. The secondary standard star used to find the (B-V) value for this system was the C3 star in that table. The (B-V) for the system was determined to be 0.65 while interstellar extinction was determined to be 0.01 leading to a final (B-V) value of 0.64. This translates to a primary star temperature of approximately 5756 K. The period of the system as determined by PERANZO is  $0.375130 \pm 0.000005$  days. The orbital inclination determined from PHOEBE was  $82.613 \pm 0.348$  degrees with a mass ratio of  $2.780 \pm 0.036$  and a secondary component temperature of  $4862 \pm 7.3$  degrees K. The average time of minimum for the system over all three filters was  $2457495.754992 \pm 0.000276$ . Figures 14-19 are the light curves and residuals in all three filters, Bessel B and V and Cousins R. Figure 27 is a 3D representation of the two stars at four positions in their orbits around one another. These four positions are at an orbital phase of 0.25, 0.5, and 0.75 of its period. Looking at the 3D representation of the stars it looks like the system is very close to being an overcontact binary. Both stars appear to be very close to the limits of their Roche lobes.

Looking at the light curves themselves it can clearly be seen that there are portions of the modeled light curves that do not match the observed light curves. These

discrepancies may be attributed to an accretion disk having formed around the primary star. However, PHOEBE is not capable of modeling a star with an accretion disk and I could not find additional literature discussing this possibility in other star systems. A second explanation for this effect is that there may be one or more starspots on the surface of the stars causing a localized temperature drop, and thus a decrease in brightness, at certain points along the light curves. Since PHOEBE is able to model starspots those are what I used to create the models of the light curves and their residuals in Figures 21-26. These figures can be compared with the models of the light curves and their residuals without starspots that can be seen in Figures 28-33. The first starspot in the model is on the primary star at a colatitude of  $110^\circ$  and a longitude of  $229^\circ$  with a radius of  $20^\circ$  and a temperature slightly higher than the area around it at 1.1 times the surrounding temperature. The second starspot for this system is on the secondary star and has a colatitude of  $100^\circ$ , a longitude of  $240^\circ$ , a radius of  $22^\circ$ , and is slightly cooler than the area around it at 0.9 times the surrounding temperature.

Looking even further at the light curves for NSVS 5060083 we can see that this object has maxima of different values. This is unlike NSVS 5354761 whose maxima were of equal heights. This is a symptom of something called the O'Connell effect. Although the exact cause of the O'Connell effect is still unknown several theories have been put forward. These include clouds of circumstellar dust and gas, a hot spot caused by the impact of a mass-transferring gas stream, asymmetrically deflected due to Coriolis forces and asymmetric distributions of starspots (O'Connell 1951). However, since the maxima following the primary eclipse is larger than that following the secondary eclipse we can

determine that this system undergoes a positive O'Connell effect. In this thesis I use starspots to compensate for this effect.

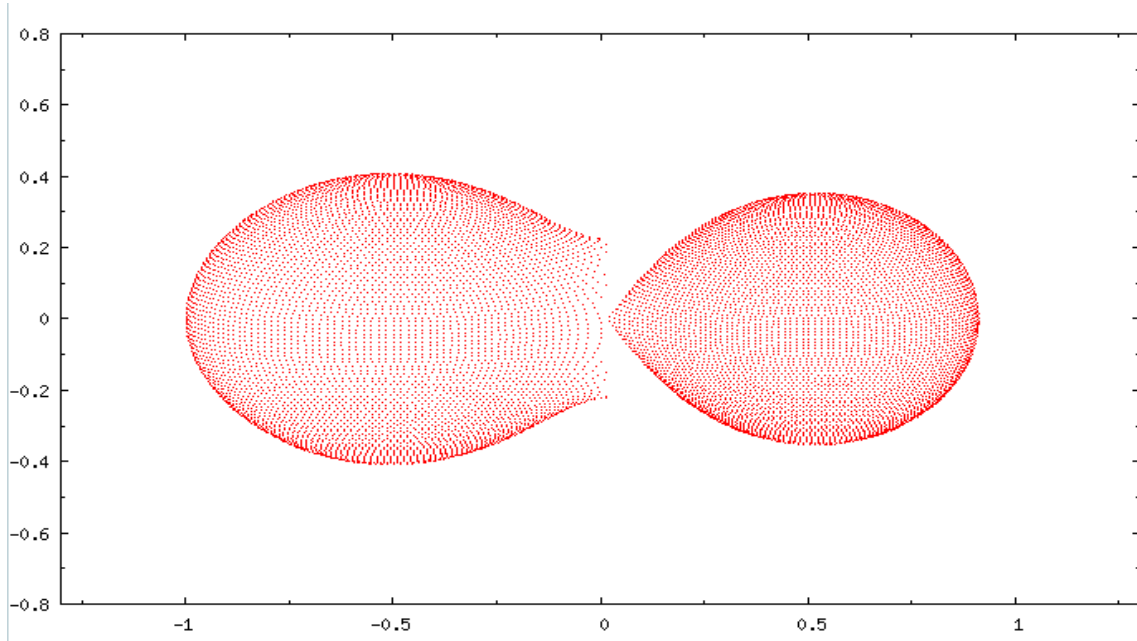


**Figure 20:** Erroneous modeling of NSVS 5060083.

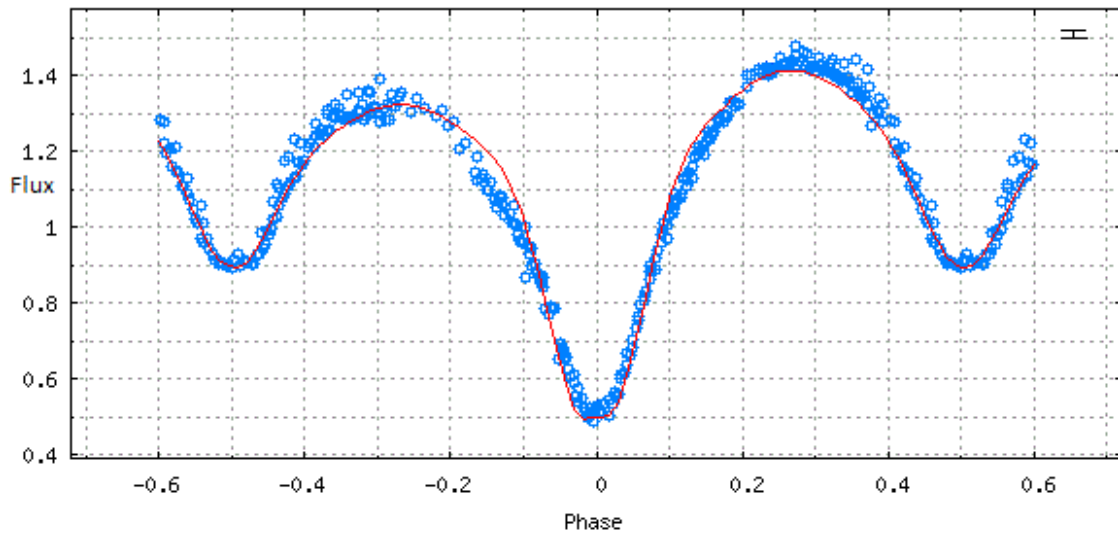


**Figure 21:** Folded light curve in Johnson B filter with starspots for NSVS 5060083. Plot of observational data (hollow circles) overlaid with the projected light curve from PHOEBE (solid curve). Error bars are omitted for clarity but a typical error bar can be seen in the upper right hand corner with a value of  $\pm 0.02$ .

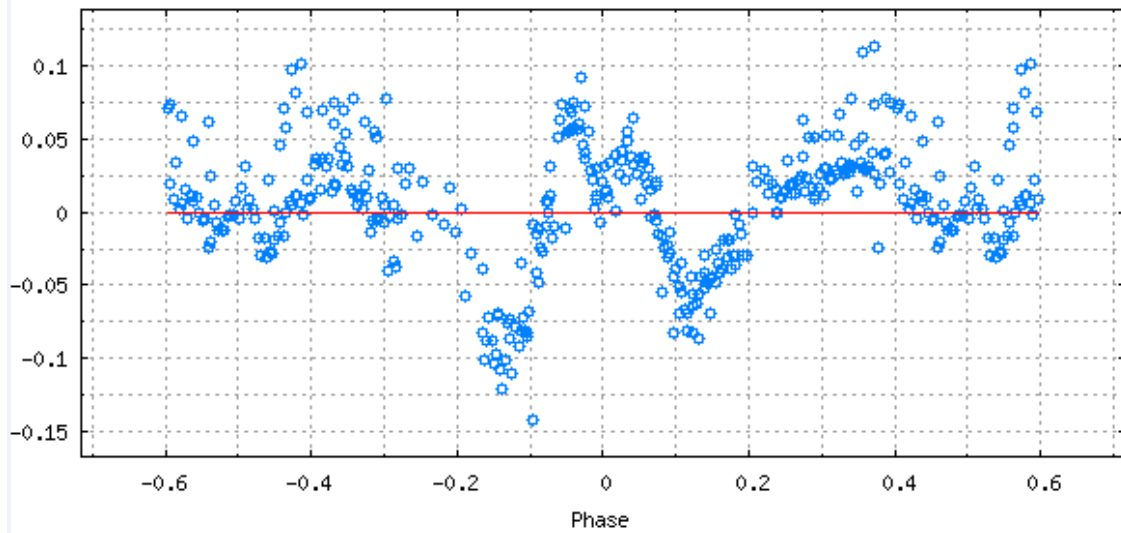


**Figure 22:** Residuals for folded light curve in Johnson B filter with starspots. Plot of the difference between the projected light curve generated from PHOEBE (solid line) and the observational data (hollow circles).

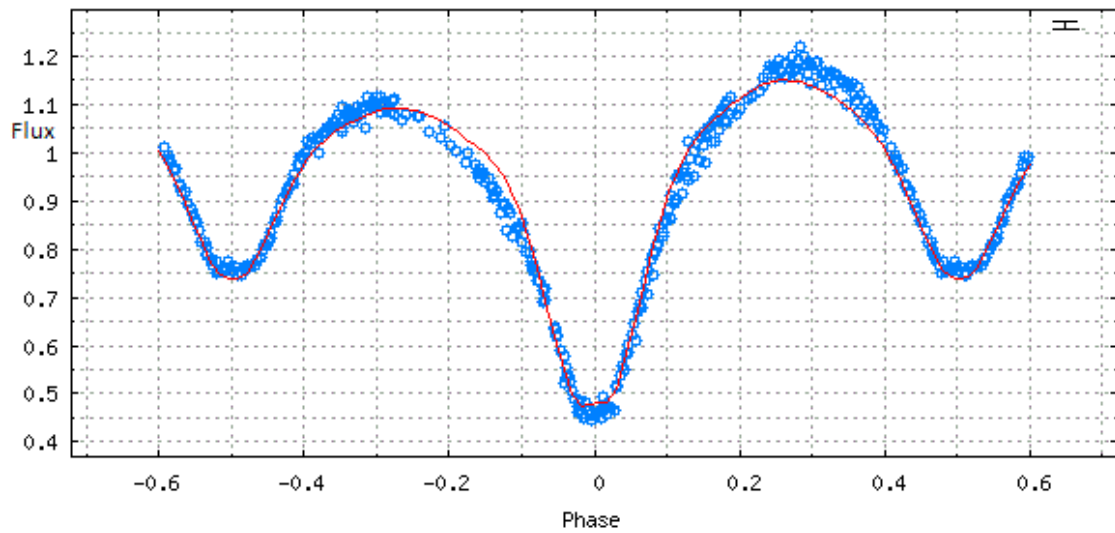


**Figure 23:** Folded light curve in Johnson V filter with starspots for NSVS 5060083. Plot of observational data (hollow circles) overlaid with the projected light curve from PHOEBE (solid curve). Error bars are omitted for clarity but a typical error bar can be seen in the upper right hand corner with a value of  $\pm 0.02$ .

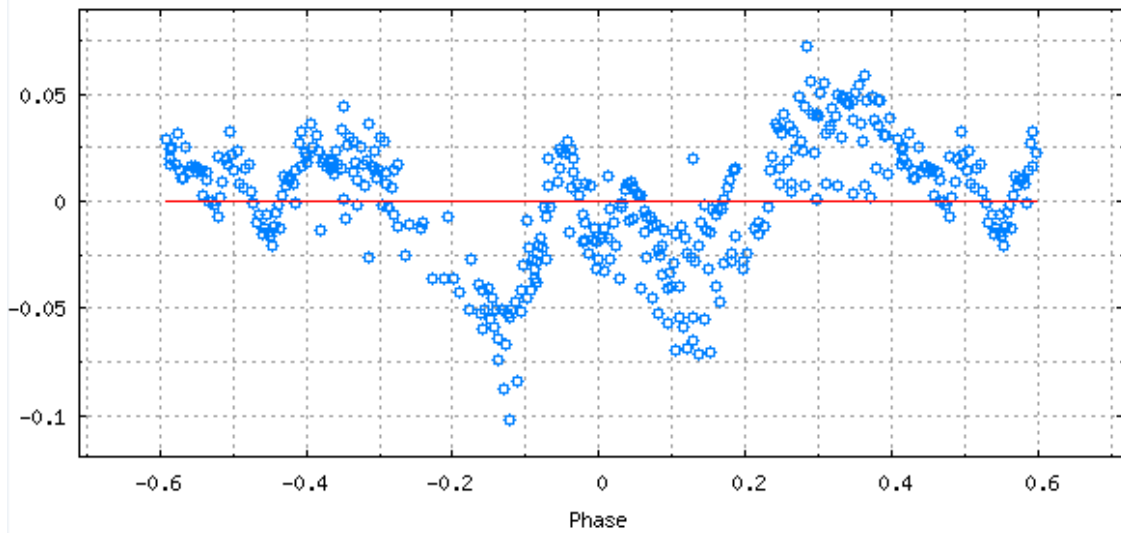


**Figure 24:** Residuals for folded light curve in Johnson V filter with starspots. Plot of the difference between the projected light curve generated from PHOEBE (solid line) and the observational data (hollow circles).

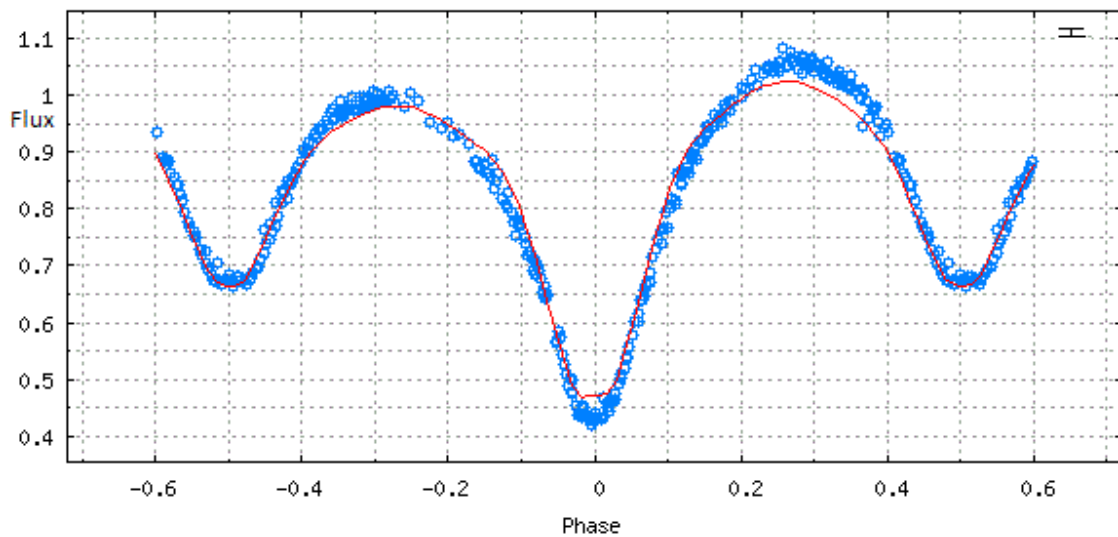


**Figure 25:** Folded light curve in Cousins R filter with starspots for NSVS 5060083. Plot of observational data (hollow circles) overlaid with the projected light curve from PHOEBE (solid curve). Error bars are omitted for clarity but a typical error bar can be seen in the upper right hand corner with a value of  $\pm 0.02$ .

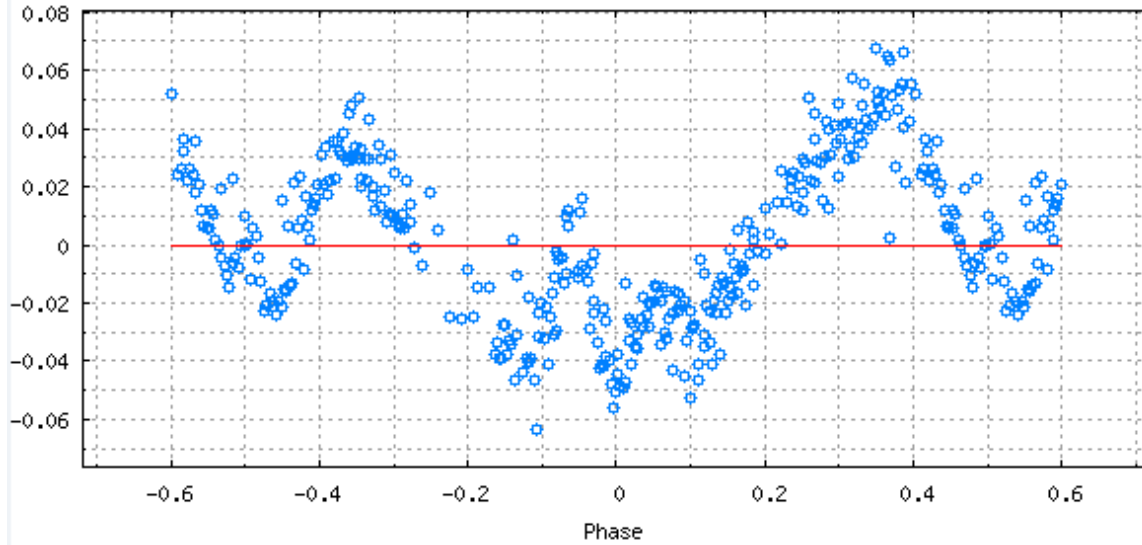


**Figure 26:** Residuals for folded light curve in Cousins R filter with starspots. Plot of the difference between the projected light curve generated from PHOEBE (solid line) and the observational data (hollow circles).

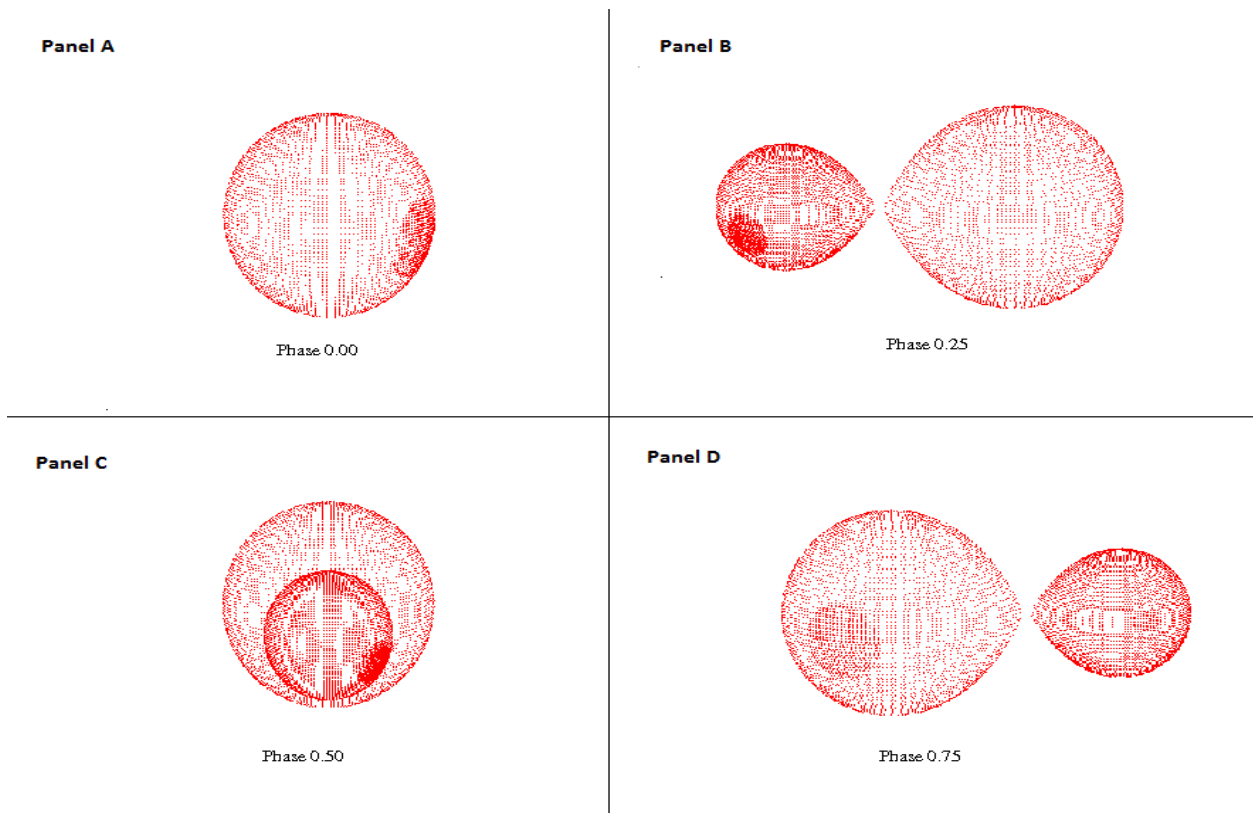


**Figure 27:** Three Dimensional Models of NSVS 5060083. . Beginning at top left with a representation of the primary eclipse (Phase 0.0) at Panel A and continuing to display the binary system at orbital phases of 0.25, 0.5 (the secondary eclipse), and 0.75 at Panels B, C, and D respectively.

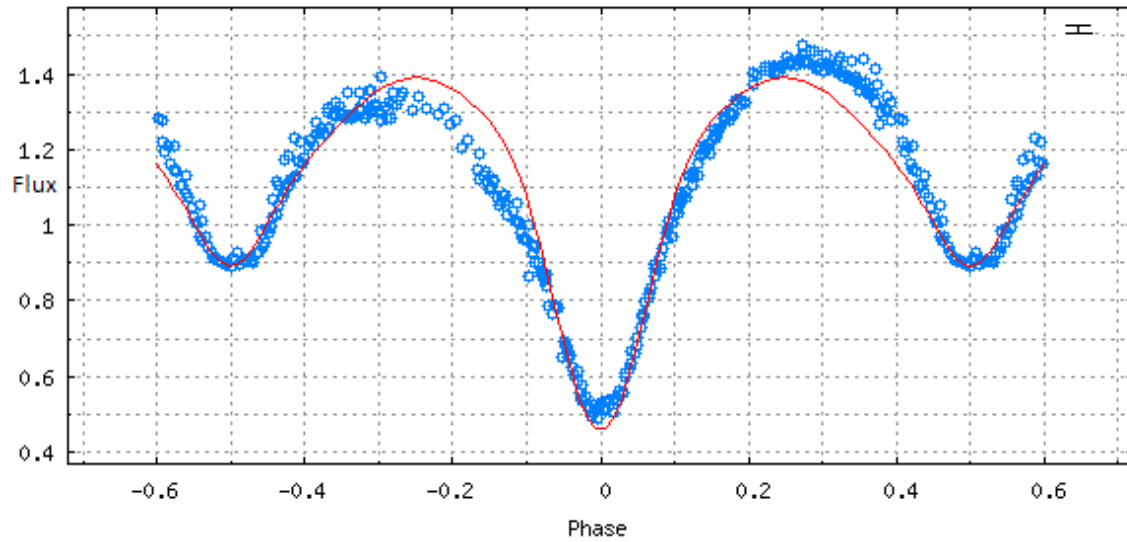


**Figure 28:** Folded light curve in Johnson B filter without starspots for NSVS 5060083. Plot of observational data (hollow circles) overlaid with the projected light curve from PHOEBE (solid curve). Error bars are omitted for clarity but a typical error bar can be seen in the upper right hand corner with a value of  $\pm 0.02$ .

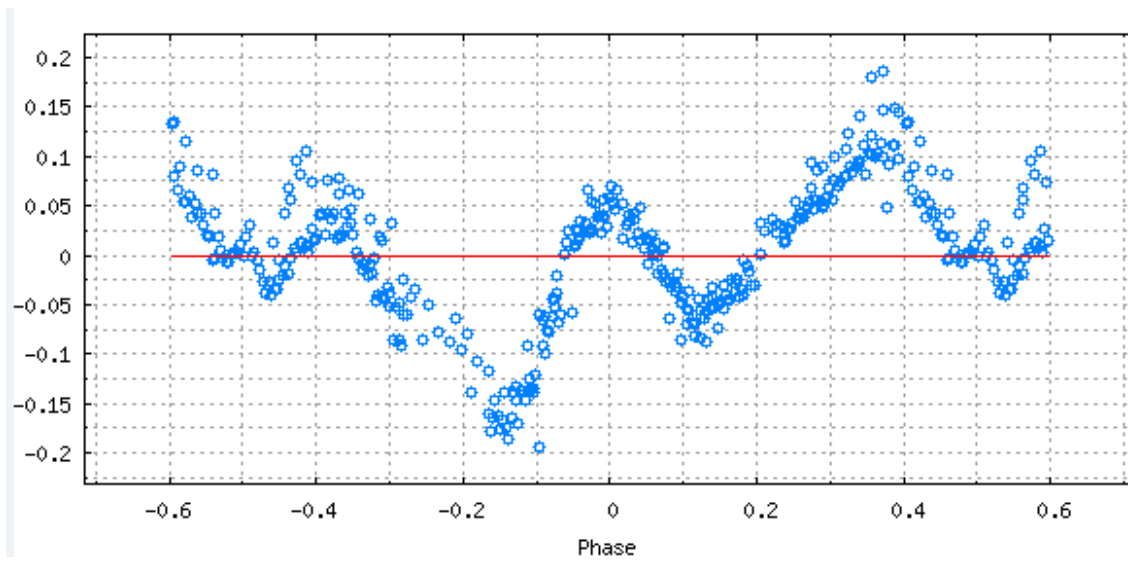


**Figure 29:** Residuals for folded light curve in Johnson B filter without spots. Plot of the difference between the projected light curve generated from PHOEBE (solid line) and the observational data (hollow circles).

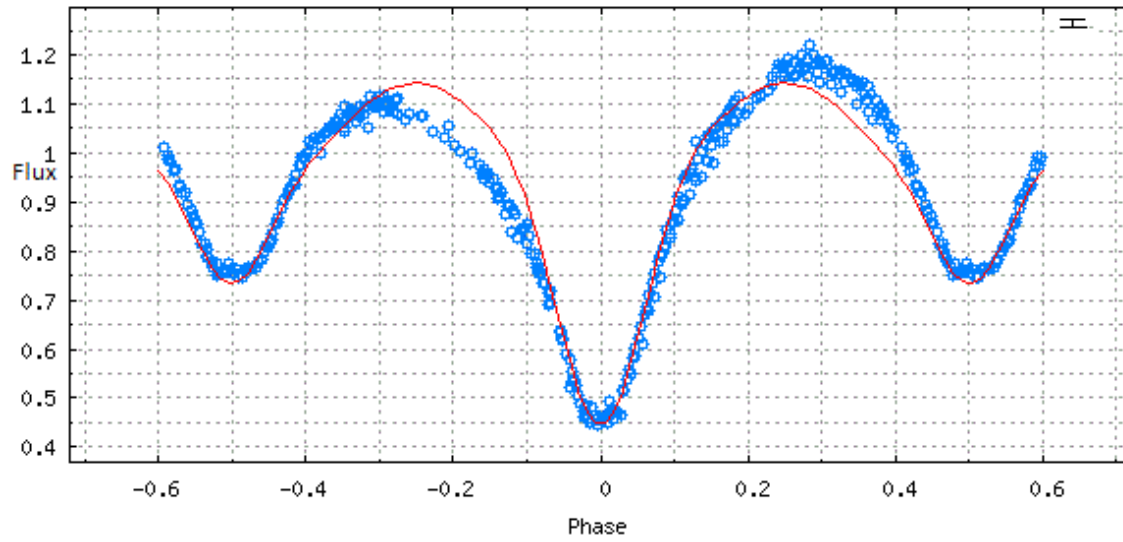


**Figure 30:** Folded light curve in Johnson V filter without starspots for NSVS 5060083. Plot of observational data (hollow circles) overlaid with the projected light curve from PHOEBE (solid curve). Error bars are omitted for clarity but a typical error bar can be seen in the upper right hand corner with a value of  $\pm 0.02$ .

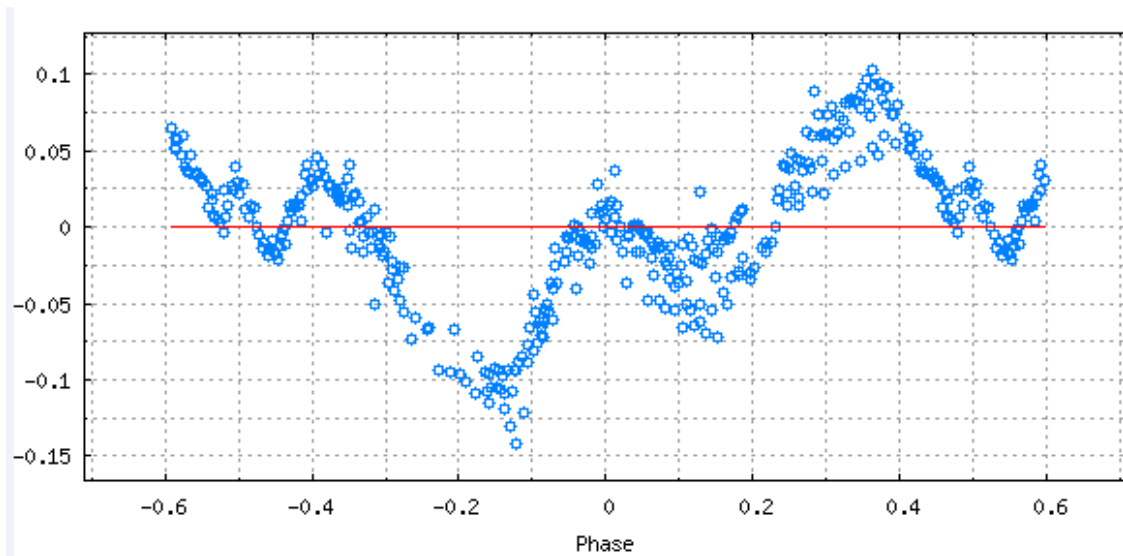


**Figure 31:** Residuals for folded light curve in Johnson V filter without spots. Plot of the difference between the projected light curve generated from PHOEBE (solid line) and the observational data (hollow circles).

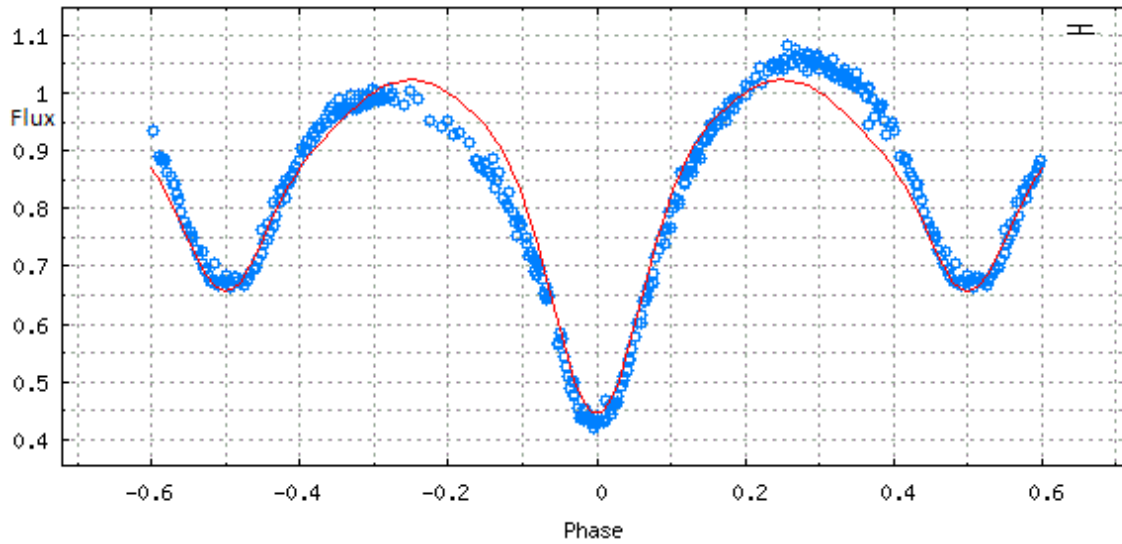


**Figure 32:** Folded light curve in Cousins R filter without starspots for NSVS 5060083. Plot of observational data (hollow circles) overlaid with the projected light curve from PHOEBE (solid curve). Error bars are omitted for clarity but a typical error bar can be seen in the upper right hand corner with a value of +/- 0.02.

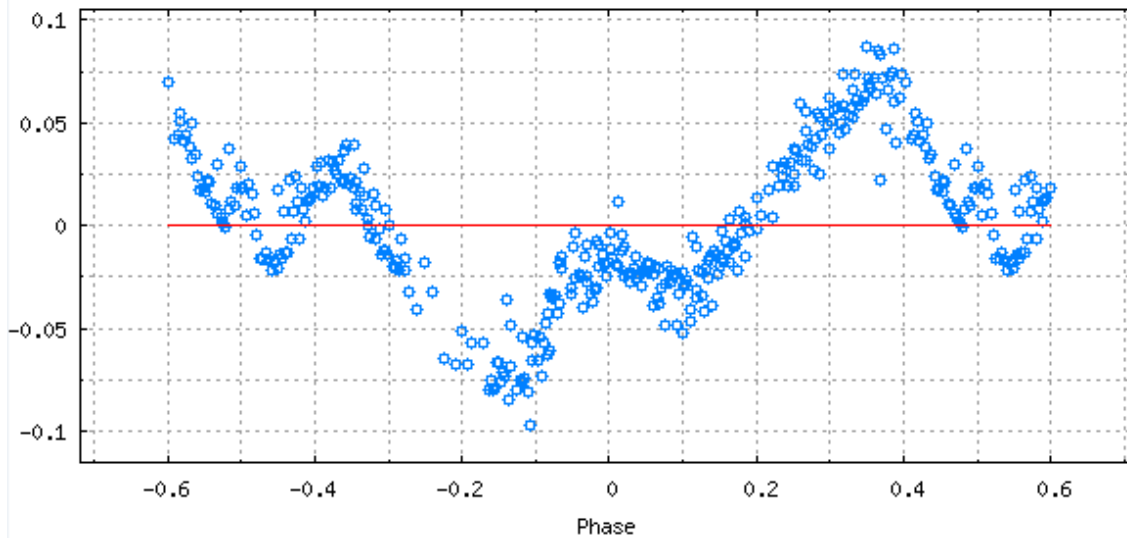


**Figure 33:** Residuals for folded light curve in Cousins R filter without spots. Plot of the difference between the projected light curve generated from PHOEBE (solid line) and the observational data (hollow circles).

Table 5 contains the final results of the modeling for both NSVS 5060083 and NSVS 5354761. These include both the set parameters needed to begin the PHOEBE modeling and the stellar parameters that could be extracted after the PHOEBE modeling was completed. The parameters set before modeling include the period of the system, the

primary star temperature, and the time of minimum for the primary eclipse. The extracted parameters include the orbital inclination and mass ratio of the system as well as the temperature of the secondary star.

	NSVS 5060083	NSVS 5354761
Period (days)	0.375130 +/- 0.000005	0.787155 +/- 0.000006
Primary Star Temperature (K)	5756	6044
Time of Minimum (HJD)	2457495.754992 +/- 0.000276	2457259.634606 +/- 0.000148
Orbital Inclination (Degrees)	82.613 +/- 0.348	78.41 +/- 0.07
Mass Ratio	2.780 +/- 0.036	1.2693 +/- 0.0094
Secondary Star Temperature (K)	4862 +/- 7.3	4976 +/- 6.7

**Table 5:** Final results from the modeling of NSVS 5060083 and NSVS 5354761.

## Chapter 6: Conclusions

Throughout this thesis I have closely examined the two star systems NSVS 5354761 and NSVS 5060083. The most difficult parts of this examination were the analysis and reduction of my images and the modeling of the systems using PHOEBE. But I can come to several conclusions about the two systems. They are both Beta Lyrae systems as shown by their continuously changing light curves that have minima of different depths during their primary and secondary eclipses. NSVS 5354761 is a detached eclipsing binary system as neither of its stellar components have completely filled their Roche lobes. This was by far the easier of the two systems to model.

NSVS 5060083 was much more difficult to model. Ultimately I determined that it was a semi-detached eclipsing binary system. However, I am not completely satisfied with the modeling of this system. The modeling was complicated by the fact that both stars appear to have almost completely filled their Roche lobes. I would also like to further

investigate the possibility that there is an accretion disk around one of the stellar components due to mass transfer. In addition, NSVS 5060083 suffers from the O'Connell effect further complicating its light curve.

I would like to continue studying these two systems in a couple of ways. First, I would like to obtain more observations for each system to further refine their light curves. Particularly, in order to discover the source of the secondary dip in the Johnson B light curve for NSVS 5354761. Second, I would like to obtain spectrographic data for both these systems in order to determine the radial velocity and masses of the individual stellar components of both systems. I was unable to do this over the course of my current research since the objects were too faint to obtain spectra from those spectrographs available for my use at this time.

## **Acknowledgements**

I would like to thank Dr. Robert Berrington for his tireless patience with and his constant availability for help and advice during the time in which I was creating this thesis. Without his constant support I'm sure this project would never have gotten done. Nor would it be as well done as it is. Much thanks also goes to Dr. Ronald Kaitchuck for helping me to understand the portions of the science that I was unfamiliar with and bringing my attention to parts of my models that I might have missed. I would also like to thank Dr. David Grosnick whose attention to detail helped greatly with formatting and helped me to understand that sometimes the most thorough explanation has to come with an image attached. I would also like to thank my colleagues Matthew Knote, Monique Gabb, and Jon Van de Water whose support both in regards to my research and outside it helped me to carry on. Thank you all very much.

## References

- Bhattacharyya, S., *Curr. Sci.*, 97, 804-820, (2009).
- Berry, R.; Burnell, J., The Handbook of Astronomical Image Processing, (Willmann-Bell Inc 2011).
- CBA Belgium Observatory, Flanders, Belgium (<http://www.cbabelgium.com>) (2011).
- Flower, P., *Astrophys. J.*, 469, 355-365, (1996).
- Kwee, K. K., van Woerden, H., *Bull. Astron. Inst. Netherlands*, 12, 327, (1956).
- Hoffman, D. I., et al., *Astron. J.*, 136, 1067, (2008).
- O'Connell, D. J. K., *Publications of the Riverview College Observatory*, 2, 85, (1951).
- Percy, J. R., Understanding Variable Stars, (Cambridge University Press 2011).
- Prsa, A., PHOEBE Scientific Reference (2011).
- Schlafly, E. F., Finkbeiner, D. P., *Astrophys. J.*, 737, 103, (2011).
- Schwarzenberg-Czerny, A., *Astrophys. J.*, 460, L107, (1996).
- Szymanski, M. K., *Acta Astronomica*, 55, 43, (2005).
- Torres, G., *Astron. J.*, 140, 1158-1162, (2010).
- Wilson, R. E.; Devinney, E. J., *Realization of Accurate Close-Binary Light Curves: Application to MR Cygni*, *Astrophys. J.*, 166, 605, (1971).
- Wozniak, P., et al., *Astron. J.*, 127, 2436-2449, (2004).